Suppression of progesterone by influenza A virus causes adverse maternal and fetal outcomes in mice

Patrick S. Creisher[1], Maclaine A. Parish[1], Jun Lei [2], Jin Liu[3], Jamie L. Perry[1], Ariana D. Campbell[1], Morgan L. Sherer[1], Irina Burd[2], and Sabra L. Klein[1,†]

[1]W. Harry Feinstone Department of Molecular Microbiology and Immunology, The Johns Hopkins Bloomberg School of Public Health, Baltimore, Maryland, USA

[2]Department of Obstetrics, Gynecology & Reproductive Sciences, University of Maryland School of Medicine, Baltimore, Maryland, USA

[3]Integrated Research Center for Fetal Medicine, Department of Gynecology and Obstetrics, Johns Hopkins University School of Medicine, Baltimore, Maryland, USA

[†]To whom correspondence should be addressed: Sabra L. Klein (sklein2@jhu.edu)

Short title: influenza and pregnancy

Key words: cytokine storm, macrophages, placenta, pregnancy, prostaglandins, progestins

Manuscript statistics:

Abstract: 138
Text: 6563
Figures: 7
References: 89

Abstract:

Influenza A virus infection during pregnancy can cause adverse maternal and fetal outcomes, but the mechanism responsible remains elusive. Infection of outbred mice with 2009 H1N1 at embryonic day (E) 10 resulted in significant maternal morbidity, placental tissue damage and inflammation, fetal growth restriction, and developmental delays that lasted through weaning. Restriction of pulmonary virus replication was not inhibited during pregnancy, but infected dams had suppressed circulating and placental progesterone (P4) concentrations that were caused by H1N1-induced upregulation of pulmonary cyclooxygenase (COX)-1, but not COX-2-, dependent synthesis and secretion of prostaglandin (PG) F2α. Treatment with 17-α-hydroxyprogesterone caproate (17-OHPC), a synthetic progestin that is safe to use in pregnancy, ameliorated the adverse maternal and fetal outcomes from H1N1 infection and prevented placental cell death and inflammation. These findings highlight the therapeutic potential of progestin treatments for influenza during pregnancy.

1 Introduction

Pregnant individuals are at increased risk of severe disease and death following infection with seasonal and pandemic influenza viruses (Cox et al., 2006; Klein et al., 2010; Mertz et al., 2017; Vousden et al., 2021; Woolston and Conley, 1918). For example, pregnancy was associated with an 18.1% increase in one hospital's fatality rate during the 1918 H1N1 pandemic and a disproportionally greater percentage of morbidity and death during the 2009 H1N1 pandemic (Klein et al., 2010; Woolston and Conley, 1918). Further, seasonal influenza viruses are reported to annually infect between 483 and 1097 per 10,000 pregnant women (Katz et al., 2017), with greater odds of adverse outcomes, including intensive care unit (ICU) admission, acute cardiopulmonary morbidity, and increased hospital length of stay, among pregnant than nonpregnant people (Cox et al., 2006; Neuzil et al., 1998; Vousden et al., 2021). In the absence of vertical transmission, influenza virus infection during pregnancy is still associated with adverse perinatal and fetal outcomes (Hartel et al., 2016; He et al., 2017; Omer et al., 2011), as was seen during the 2009 H1N1 pandemic, where maternal influenza A virus (IAV) infection increased the relative risk of low birth weights and stillbirths by 71% and 136%, respectively (He et al., 2017). Moreover, infection with influenza viruses during pregnancy has been associated with long-lasting consequences for offspring, such as increasing the risk of development of neuropsychiatric and metabolic disorders in adulthood (Brown et al., 2004; Parboosing et al., 2013; Song et al., 2020).

The 2009 H1N1 pandemic spurred development of mouse models of IAV infection during pregnancy to uncover mechanisms of adverse maternal and fetal outcomes. Collectively, these studies have revealed pregnancy-specific mechanisms of influenza pathogenesis. Notably, pregnant mice infected with diverse influenza viruses consistently experience greater morbidity and/or mortality than nonpregnant female mice, consistent with observations in humans (Chan et al., 2010; Engels et al., 2017; Kim et al., 2012; Littauer et al., 2017; Marcelin et al., 2011;

Pazos et al., 2012). Pregnancy impacts pulmonary innate immune activity and tissue repair following IAV infection, as pregnant dams have greater proinflammatory cytokine concentrations and numbers of neutrophils and macrophages in lungs than nonpregnant females (Chan et al., 2010; Engels et al., 2017; Lauzon-Joset et al., 2019; Marcelin et al., 2011; Pazos et al., 2012). Moreover, IAV infection during pregnancy is associated with pulmonary tissue damage, impaired epithelial regeneration, reduced progesterone (P4) concentrations, and a shift of alveolar macrophages from a classical to an alternative activation state (Lauzon-Joset et al., 2019; Marcelin et al., 2011; Swieboda et al., 2020; Vermillion et al., 2018). Pregnant dams infected with IAV have reduced adaptive immune responses including reduced IAV-specific antibody titers, numbers of circulating $CD4^+$ and $CD8^+$ T cells, and IAV-specific cytotoxic T cell activity, with these effects associated with changes in circulating P4 and estrogens (Chan et al., 2010; Engels et al., 2017; Peluso et al., 1980; Swieboda et al., 2020). Whether IAV-induced changes in circulating concentrations of sex steroids are a cause or consequence of maternal disease during infection has not been determined.

Although mice do not recapitulate all aspects of human pregnancy, mice do exhibit many of the cardiovascular, hormonal, and immunological changes associated with pregnancy (Abu-Raya et al., 2020; Ander et al., 2019; Arany et al., 2022; Krishnan et al., 2013; Malassine et al., 2003). For example, concentrations of P4 increase dramatically during pregnancy and support the growth of the placenta in both mice and humans (Di Renzo et al., 2016; Malassine et al., 2003), with secretion exclusively by the corpus luteum in mice and secretion shifting from the corpus luteum to the placenta mid-gestation in humans (Malassine et al., 2003; Terakawa et al., 2012). Mouse models of pregnancy have limitations, including shorter gestation in mice and distinct mechanisms of placentation (Arany et al., 2022; Krishnan et al., 2013; Malassine et al., 2003). Furthermore, when using inbred mice, the absence of a semi-allogeneic fetus limits tolerogenic immune mechanisms observed in humans and outbred animals (Moldenhauer et al.,

2010; Tafuri et al., 1995), which has been shown to contribute to IAV pathogenesis (Engels et al., 2017; Jacobsen et al., 2021).

In the current study, using outbred mice, IAV infection during pregnancy caused significant maternal morbidity and adverse fetal outcomes that were associated with transient placental tissue damage and inflammation. Both maternal disease and adverse perinatal outcomes were mediated by IAV-induced activation of cyclooxygenase-1 (COX-1), but not COX-2, causing increased activation of prostaglandin F2α (PGF2α) and suppression of P4. Treatment of IAV-infected pregnant female mice with a synthetic progestin that is safe for administration during pregnancy reversed the adverse maternal, placental, and fetal outcomes from IAV infection. This novel study highlights utilizing hormone modulating treatments for the treatment of influenza during pregnancy.

2 Materials and Methods

2.1 Viruses and cells

Viral seed stocks of mouse adapted A/California/04/09 H1N1 (maH1N1), generated by reverse genetics from a published sequence (Ye et al., 2010) were kindly provided by Dr. Andy Pekosz (Johns Hopkins University). Working stocks were generated by infecting Madin-Darby canine kidney (MDCK) cells at a multiplicity of infection (MOI) of 0.01 tissue culture infectious dose 50 ($TCID_{50}$) per cell in infection media [DMEM (Sigma D5796) supplemented with 0.5% filter-sterilized bovine serum albumin (BSA; Sigma A9647), 100 U/mL penicillin and 100 µg/mL streptomycin (Gibco 15149–122), 2 mM l-glutamine (Gibco 25030–081), and 5 µg/mL of N-acetyl trypsin (Sigma T6763)]. Approximately 72 h post infection, the supernatant fluids were collected, clarified by centrifugation (500 g for 10 minutes), and stored in aliquots at –70°C.

2.2 Experimental mice

Timed-pregnant adult (8–12 weeks of age) CD-1 IGS mice were purchased from Charles River Laboratories. Animals arrived at embryonic day 8 (E8) and were singly housed under

standard biosafety level 2 housing conditions with ad libitum food and water. Pregnant mice were acclimated for at least 24 h prior to infections (Creisher et al., 2022a). Monitoring and procedures for animal experiments were performed consistently at the same time of day.

2.3 IAV infections and monitoring

Pregnant dams were intranasally infected at E10 with 10^3 $TCID_{50}$ units of maH1N1 in 30 µl of media (DMEM; Sigma D5796), a sublethal dose in nonpregnant CD-1 female mice, or mock inoculated with 30 µl of media. Prior to intranasal infection, mice were anesthetized via intraperitoneal ketamine/xylazine cocktail (80 mg/kg ketamine, 5 mg/kg xylazine). Following intranasal infections, body mass and rectal temperature were monitored once daily in the morning for 14 days or until tissue collection.

2.4 COX inhibitor treatments

Experimental animals were administered vehicle alone [20% DMSO (Sigma D2650) v/v diluted in PBS], the COX-1 specific inhibitor SC-560 (10 mg/kg; abcam ab120649), or the COX-2 specific inhibitor NS-398 (10 mg/kg; MedChemExpress HY-13913) in 100 µl intraperitoneally (Futaki et al., 1993; Tanigawa et al., 2004; Thomas and Kuhn, 2005). Mice were administered treatment twice daily, starting 1 day prior to infection and until tissue collection at 3 dpi. Serum thromboxane B2 was measured to confirm COX-1 inhibition (Wallace et al., 1998; Wallace et al., 1999) by ELISA per the manufacturer's instructions (Cayman Chemical 19030). Inhibitors were reconstituted and diluted fresh for each dose.

2.5 17α-hydroxyprogesterone caproate treatment

17α-hydroxyprogesterone caproate (17-OHPC, 250 mg/mL) was obtained from the Johns Hopkins Hospital Pharmacy (NDC 71225-105-01) and diluted to 20 mg/mL in vehicle [46% v/v benzyl benzoate (Sigma B6630) in castor oil (Sigma C9606)]. Experimental animals were administered vehicle alone or 17-OHPC subcutaneously at the time of intranasal infection. 17-OHPC was administered at a dose of 2 mg/dam, which previously demonstrated efficacy in

preventing adverse neurological outcomes in a mouse model of intrauterine inflammation (Novak et al., 2018), and was administered as a single injection due to the prolonged half-life of 17-OHPC when delivered in an oil-based solution [>7 days (Shaik et al., 2016)].

2.6 Offspring measurements and developmental assessments

Offspring from IAV- and mock-inoculated dams were measured at post-natal day (PND) 0, within 12 hours of birth. Body mass (g), length measured from nose to anus (mm), and head diameter measured from ear to ear (mm) were recorded for each pup, using a caliper, and the average for each independent litter was calculated to avoid confounding litter effects. After birth and until weaning, pups were monitored daily for body mass (g) and the appearance of key developmental milestones including fur development, the opening of the ear canals and eyes, and teeth eruption (Heyser, 2004; Hill et al., 2008). At PND5, pups were subjected to the developmental neurobehavioral assay of surface righting, as described (Creisher et al., 2023; Feather-Schussler and Ferguson, 2016). For each test, 1–2 male and 1–2 female offspring from at least 5 independent litters were used per condition to avoid confounding litter effects. Pups were subjected to 3 attempts, with the time to complete the test recorded on a stopwatch. The upper limit of time was 60 seconds, and a pups' best trial for each test was used for analysis.

2.7 Tissue and serum collection

Experimental mice were euthanized via ketamine/xylazine overdose (160 mg/kg ketamine, 10 mg/kg xylazine) followed by cardiac exsanguination at 1, 3, 6, or 8 days post-infection. Maternal lungs, spleen, and ovaries were collected and flash frozen on dry ice for homogenization. Fetuses and placenta were flash frozen in dry ice or fixed in 4% paraformaldehyde (Thermo Fisher Scientific J19943.K2) for 72 h at 4°C for immunohistochemistry. Serum was separated from blood by centrifugation at 10,000 rpm for 30 min at 4°C.

2.8 Tissue homogenization and infectious virus quantification

Frozen right cranial lungs, spleen, ovaries, placentas, and fetuses were weighed and homogenized in 1:10 weight per volume of PBS using Lysing Matrix D tubes (MP Biomedicals #6913100) in a MP Fast-prep 24 5G instrument. Homogenate was clarified by centrifugation at 12,000 rpm and stored at -70°C until analysis. IAV infectious virus titers in tissue homogenate was determined by $TCID_{50}$ assay, as described previously (Hall et al., 2017; Vermillion et al., 2018). Briefly, tissue homogenates were serially diluted in infection media and plated onto a monolayer of 100% confluent MDCK cells in replicates of 6. Cells were incubated for 7 days at 32°C and 5% CO2, fixed for 1 hour with 4% formaldehyde, and then stained with naphthol blue black for 4 hours. After staining, plates were scored for cytopathic effects and the Reed-Muench method was used to calculate the $TCID_{50}$ titer for each sample.

2.9 Multiplex cytokine analysis

Cytokines and chemokines in the right cranial lung, spleen, and placenta homogenate were multiplexed using the Immune Monitoring 48-Plex Mouse Procartaplex Panel (Thermo Fisher Scientific EPX480-20834-901) miniaturized with the Curiox DA-Bead DropArray platform (Versteeg et al., 2017). Briefly, 96-well DA-Bead Plates (Curiox 96-CC-BD-05) were blocked with 10 µL per well of 1% BSA (Sigma A9647) in PBS for 30 min in a humidified magnet box (Curiox HMBXWT01) at room temperature on a rotator. The plate was washed with Curiox wash buffer [0.1% BSA (Sigma A9647) and 0.05% Tween-20 (Sigma P1379)] on a DropArray LT210 (Curiox). Procartaplex beads (5 µL) were added to each well, followed by 5 µL of serially diluted ProCartaplex standards or 10 µL tissue homogenate per well, with each sample assayed in duplicate. The plate was incubated overnight in a humidified magnet box on a rotator at 4°C. The following day, the plate was washed three times, and 5 µL of ProCartaPlex detection antibody added per well. The plate was incubated for 1 h in a humidified magnet box on a rotator. After incubation, 10 µL streptavidin-phycoerythrin was added to each well and incubated for 30 min in a humidified magnet box on a rotator. The plate was washed three times, and the

beads were reconstituted in Curiox wash buffer and transferred to a skirted v-bottom 96 well plate (Biorad HSP9601) for reading on a MagPix system (Luminex). Analysis was performed using BioPlex Manager (version 6.2). The following analytes were quantified: G-CSF, GM-CSF, M-CSF, CXCL1, CXCL2, CXCL5, CXCL10, CCL2, CCL3, CCL4, CCL5, CCL7, CCL11, IFNα, IFNγ, IL-1β, IL-1α, IL-2, IL-3, IL-2R, IL-4, IL-5, IL-6, IL-7, IL-7Rα, IL-9, IL-10, IL-12p70, IL-13, IL-15/IL-15R, IL-17A IL-18, IL-19, IL-22, IL-23, IL-25, IL-27, IL-28, IL-31, IL-33, IL-33R, Leukemia inhibitory factor (LIF), TNFα, receptor activator of nuclear factor kappa-B ligand (RANKL), B-cell activating factor (BAFF), Betacellulin, vascular endothelial growth factor (VEGF-A), and Leptin.

2.10 Placental histology, immunohistochemistry, and TUNEL staining

Placentas were fixed overnight at 4°C in 4% PFA and were washed five times with PBS and immersed in 30% sucrose until saturation. Using a Leica CM1950 cryostat, the specimens were cut at 20-μm thickness and mounted on positively charged slides (Fisher Scientific12-550-15). Routine H&E staining was performed to evaluate the morphological change of the placentas. For immunohistochemical staining, slides were washed with PBS, followed by permeabilization in PBS solution containing 0.05% Triton X-100 and 10% normal goat serum (ThermoFisher Scientific 50197Z) for 30 min. Placentas were incubated with rabbit anti-vimentin (1:200, Abcam ab92547) or rabbit anti-cytokeratin (1:200, Dako Z0622) overnight at 4°C. The next day, sections were rinsed with PBS and incubated with donkey anti-rabbit (ThermoFisher Scientific R37119) fluorescent secondary antibodies diluted 1:500 for 3 h at room temperature. DAPI (Roche 10236276001) was applied for counterstaining, followed by mounting with Fluoromount-G (eBioscience 00-4958-02). Images were taken using a Zeiss Axioplan 2 microscope (Jena) under 5x or 20x magnification. Cell density of vimentin and cytokeratin positive cell quantification was performed using Image J (1.47v). The 20x images were captured from the same batch of experiments, utilizing identical imaging parameters, including exposure time for quantification. After setting the appropriate scale and threshold for positive expression,

the percentage of positive expression relative to the entire area was calculated. For each placenta, six random images in the labyrinth at the middle level (thickest) of placenta were taken, and the average fluorescent area calculated for that placenta. One placenta per dam was used and 5-10 dams per group were analyzed. Terminal deoxynucleotidyl transferase dUTP nick end labeling (TUNEL) was performed with Click-iT™ Plus TUNEL Assay (ThermoFisher C10617) per the manufacturer protocol. Placental slides were fixed with 4% paraformaldehyde in PBS for 15 min at 37°C, rinsed with PBS, and permeabilized with proteinase K solution for 15 min at RT followed by staining with TUNEL working solution for 60 min at 37°C. Specimens were mounted on glass slides using Fluoromount-G (eBioscience #00-4958-02). For each placenta, 10 random images in labyrinth at the middle level (thickest) of placenta were taken, and the average percentage $TUNEL^+$ ($TUNEL^+$ fluorescent signal divided by the DAPI fluorescent signal) given for that placenta. One placenta per dam was used and 5-9 dams per group were analyzed.

2.11 Flow cytometry

Placentas and maternal blood were collected from a subset of experimental dams at 6 dpi for flow cytometry as described previously (Liu et al., 2021; Liu et al., 2022). Single cells were prepared from 3 pooled placentas per dam. Manual digestion was performed by mincing placentas into 2-4 mm pieces using a scalpel blade on ice, followed by enzymatic digestion with collagenase D (Roche 11088882001) in 6 mL of Hanks' Balanced Salt Solution with calcium and magnesium (HBSS+; Gibco 14025-092) at 37℃. Collagenase D digestion was stopped after 30 min with 6 mL of Hanks' Balanced Salt Solution without calcium and magnesium (HBSS-; Gibco 14175-095), and cells were passed through a 70 µm nylon mesh cell strainer and washed with HBSS- thrice. Red blood cell lysis with ACK lysing buffer (Quality Biological 118-156-101), Fc blocking [anti-CD16/32 (BD Biosciences 554142)], and total cell counts were performed prior to resuspension in cell staining buffer [0.5% BSA (Sigma A9647) + 0.05%

sodium azide (Sigma S8032) + 1mM EDTA (Quality Biological 351-027-101) in PBS] for staining. Maternal blood (1 mL) was added to 10 ml of 5 mM EDTA (Quality Biological 351-027-101) in HBSS+ (Gibco 14175-095), followed by centrifugation at 300g for 5 min at 4℃, red blood cell lysis with ACK lysing buffer, Fc blocking, total cell counts, and resuspension in cell staining buffer for staining. Single cell suspensions were split in half and stained with one of two surface marker antibody cocktails at 1:100 for 30 min on ice in the dark. Panel one contained anti-mouse CD45 (clone 30-F11) Super Bright 600 (Thermo Fisher Scientific 63-0451-82), anti-mouse CD11b (clone M1-70) PerCP-Cyanine5.5 (Thermo Fisher Scientific 45-0112-82), anti-mouse F4/80 (clone BM8) eFluor 450 (Thermo Fisher Scientific 48-4801-82), anti-mouse CD170 (clone 1RNM44N) PE-Cyanine7 (Thermo Fisher Scientific 25-1702-82), anti-mouse CD163 (clone TNKUPJ) PE (Thermo Fisher Scientific 12-1631-82), and anti-mouse CD68 (clone FA-11) Alexa Fluor 488 (Thermo Fisher Scientific 53-0681-82). Panel two contained anti-mouse CD45 (clone 30-F11) PE (Thermo Fisher Scientific 12-0451-82), anti-mouse NK1.1 (clone PK136) PE-Cyanine7 (Thermo Fisher Scientific 25-5941-82), anti-mouse CD3 (clone 17A2) eFluor 450 (Thermo Fisher Scientific 48-0032-82), anti-mouse CD8a (clone 53-6.7) eFluor 506 (Thermo Fisher Scientific 69-0081-82), and anti-mouse CD19 (clone eBio1D3) Super Bright 600 (Thermo Fisher Scientific 63-0193-82). After incubation, cells were washed and acquired on acquired on an Attune™ NxT Acoustic Focusing Cytometer (ThermoFisher Scientific) and analyzed with FlowJo (version 10.8.1). Compensation was performed with OneComp eBeads (Thermo Fisher Scientific 01-1111-41). Gating was performed as described previously [(Liu et al., 2021; Liu et al., 2022) and **Supplemental Fig. 3**]. Debris and doublets were excluded by gating on side scatter height versus side scatter area to delaminate singlets, and specific populations including leukocytes, ($CD45^+$), NK cells ($CD45^+$, $CD3^-$,$CD19^+$), B cells ($CD45^+$, $CD3^-$,$CD19^+$), $CD4^+$ T cells ($CD45^+$, $CD3^+$, $CD4^+$), $CD8^+$ T cells ($CD45^+$, $CD3^+$, $CD8a^+$), neutrophils ($CD45^+$, $CD11b^+$, $F4/80^-$, $CD170^-$, side scatter area high), eosinophils ($CD45^+$,

CD11b$^+$, F4/80$^+$, CD170$^+$), CD163$^+$ macrophages (CD45$^+$, CD11b$^+$, F4/80$^+$, CD163$^+$), and CD68$^+$ macrophages (CD45$^+$, CD11b$^+$, F4/80$^+$, CD68$^+$) were gated based on unstained and fluorescent minus one (FMO) controls.

2.12 Progesterone and prostaglandin ELISA

To measure P4, steroids were extracted from 50 µL of serum or tissue homogenate via diethyl ether extraction at a 1:5 sample to ether ratio. Extracted steroids were diluted 1:100 (serum) or 1:10 (tissue homogenate) and P4 was quantified by ELISA according to the manufacturer's instructions (Enzo Life Sciences ADI-900-11). PGF2α (Alpco 74-PGFHU-E01) and PGE2 (Alpco 74-PG2HU-E01) in serum or tissue homogenate was quantified by ELISA according to the manufacturer's instructions.

2.13 Western Blot

Flash frozen right caudal lung lobes and right ovaries were homogenized in 1X Cell lysis Buffer (Cell Signaling Technology 9803) with 1X Protease Inhibitor cocktail (Sigma-Aldrich P8340) and sodium fluoride (Fisher Scientific S299; 20µL lysis buffer per mg tissue). Protein lysates were stored at -80°C until analysis. Protein concentration of each lysate was measured using the Pierce BCA Protein Assay Kit. For each sample, 20 µg of protein was subjected to sodium dodecyl sulfate-polyacrylamide gel electrophoresis (SDS-PAGE) on NuPAGE 4-12% Bis-Tris gels. The gel was blotted onto Immobilon-FL PVDF Membrane (Millipore #IPFL00010) and the membranes were blocked with a 1:1 mixture of 1XPBS/Tween-20 solution (Sigma-Aldrich P3563) and Intercept blocking buffer (LI-COR Biosciences 927-70001) for 30 min at room temperature. Membranes were treated with a primary antibody diluted in blocking solution at 4°C overnight on a rocker. Membranes were then washed with PBS-Tween three times and incubated in secondary antibody solutions for one hour at room temperature on a rocker. Membranes were washed three times in PBS-Tween and then imaged on an Azure 600 imager (Azure Biosystems). Individual bands were quantified using Image Studio software (LI-COR

Biosciences; version 3.1.4) The signal from each band was normalized against the GAPDH signal and graphed as arbitrary units. Primary antibodies used were rabbit anti-COX-1 (abcam ab109025), rabbit anti-COX-2 (abcam ab179800), and mouse anti-GAPDH (abcam ab82450). Secondary antibodies included goat anti-mouse Alexa Fluor 488 (Thermo Fisher Scientific A11001) and donkey anti-rabbit Alexa Fluor Plus 647 (Thermo Fisher Scientific A32795).

2.14 Statistical analyses

Body mass change and rectal temperature were plotted and the area under the curve (AUC) was calculated to provide individual data points that captured change over time, with AUCs compared with either two tailed unpaired t-test or two-way analysis of variance (ANOVA) followed by *post-hoc* Bonferroni multiple comparisons test. Viral titers in lungs from infected dams were analyzed using one-way or two-way ANOVA followed by *post-hoc* Bonferroni multiple comparisons test. Multiplex cytokine quantifications were analyzed using multiple unpaired t-tests with Holm-Šídák correction for multiple comparisons or two-way ANOVA followed by *post-hoc* Bonferroni multiple comparisons test. Developmental milestones were analyzed using Mann-Whitney test or Kruskal-Wallis test followed by *post-hoc* Dun's multiple comparison test. Birth and neurodevelopment measurements, IHC quantification, and TUNEL quantification were analyzed with two tailed unpaired t-test, two-way ANOVA followed by *post-hoc* Bonferroni multiple comparisons test, or three-way ANOVA followed by *post-hoc* Bonferroni multiple comparisons test. Concentrations P4, PGs, and TxB2 were analyzed with two-way ANOVA followed by *post-hoc* Bonferroni multiple comparisons test. Western blot quantification and flow cytometry quantification were analyzed with two tailed unpaired t-test. Mean or median differences were considered statistically significant at $p < 0.05$. Statistical analyses were performed using GraphPad Prism v10.0.2 (GraphPad Software).

2.15 Study approval

All animal procedures were approved by the Johns Hopkins University Animal Care and Use Committee (MO21H246).

3 Results

3.1 Influenza A virus infection during pregnancy causes a pulmonary cytokine storm and maternal morbidity in outbred mice

Mouse models of IAV infection during pregnancy primarily use inbred mice (Chan et al., 2010; Kim et al., 2012; Littauer et al., 2017; Pazos et al., 2012; Vermillion et al., 2018) that are devoid of fetal genetic heterogeneity (Engels et al., 2017; Jacobsen et al., 2021). Intranasal IAV infection of pregnant outbred CD1 mice at E10, roughly corresponding to the human second trimester (Sones and Davisson, 2016), resulted in significant morbidity, in which IAV-infected dams gained less body mass (**Fig. 1A**) and experienced hypothermia (**Fig. 1B**) relative to mock-inoculated dams. IAV-infected dams experienced greater hypothermia than nonpregnant females (**Supplemental Fig. 1A)**. Subsets of dams were euthanized at 3, 6, and 8 days post infection (dpi) to measure pulmonary infectious viral loads (**Fig. 1C**) and cytokine concentrations in lungs and spleens (**Fig. 1D, Supplemental Table 1, Supplemental Table 2**) prior to and during peak disease. Pulmonary viral load peaked at 3 dpi and was low to undetectable at 8 dpi (**Fig. 1C**), which was consistent and not significantly different from IAV-infected nonpregnant female mice (**Supplemental Fig. 1B**). Prototypical cytokines and chemokines associated with influenza (Teijaro, 2015), including interferons (IFNs), tumor necrosis factor (TNF) α, interleukin (IL)-6, and CCL2 were upregulated throughout infection in the lungs, but not the spleens of IAV-infected dams (**Fig. 1D, Supplemental Table 1, Supplemental Table 2**). Together, these data indicate that outbred pregnant mice infected with IAV experience morbidity to a greater degree than nonpregnant females and a pulmonary cytokine storm, consistent with previous studies (Chan et al., 2010; Kim et al., 2012; Vermillion et al., 2018).

3.2 Influenza A virus infection during pregnancy causes intrauterine growth restriction and postnatal developmental delays

IAV infection during pregnancy is associated with adverse fetal outcomes including pre-term delivery, fetal growth restriction, and low birthweights (Hartel et al., 2016; He et al., 2017; Omer et al., 2012; Omer et al., 2011) as well as long-term health consequences in adulthood (Mazumder et al., 2010; Song et al., 2020) in humans. In mice, IAV infection during pregnancy did not impact litter size (**Fig. 2A**) or increase the rate of stillbirths (98.78% viability) versus mock inoculated dams (98.82% viability). IAV infection of dams resulted in significant fetal growth restriction, with pups of IAV-infected dams being smaller at birth based on measures of mass, length, and head diameter, than offspring of mock-inoculated dams (**Fig. 2B-D**). Offspring of IAV-infected dams remained smaller than offspring from mock-inoculated dams through weaning (**Fig. 2E**). Offspring of IAV-infected dams also displayed developmental delays, reaching key developmental milestones (Hill et al., 2008) on average 1-2 days later than offspring of mock-inoculated dams (**Fig. 2F**). Impaired surface righting, a developmental reflex (Feather-Schussler and Ferguson, 2016; Hill et al., 2008), also was apparent, with offspring, particularly males, of IAV-infected dams taking significantly longer to right themselves (**Fig. 2G**). Fetal growth restriction and developmental delays were not caused by pre-term birth as all dams, regardless of maternal infection, delivered pups at approximately E20 (Elovitz et al., 2003). These data indicate that IAV infection of outbred mice causes both short and long-term adverse perinatal and fetal outcomes, consistent with humans (He et al., 2017; Mazumder et al., 2010).

3.3 Influenza A virus infection during pregnancy causes transient but significant placental cell death and trophoblast loss

While many models of IAV infection during pregnancy have focused on uncovering mechanisms of maternal disease (Engels et al., 2017; Marcelin et al., 2011; Pazos et al., 2012;

Swieboda et al., 2020; Vermillion et al., 2018), the mechanisms of adverse fetal outcomes remain less clear. Placental tissue damage, in the absence of direct viral infection, has been reported in mice (Chan et al., 2010; Littauer et al., 2017; Swieboda et al., 2020) and in limited observational human studies (Kanmaz et al., 2011; Meijer et al., 2014). Despite no infectious virus in the placenta (data not shown), at 3 dpi, there was significant placental damage, including mixing of maternal and fetal red blood cells (**Fig. 3A**), suggestive of disruption of the placental trophoblast-endothelial cell barrier, as well as increased cell death as compared with placentas from mock-inoculated dams (TUNEL$^+$ cells, **Fig. 3B** for representative image, **Fig. 3E** for quantification). Staining for cytokeratin (trophoblasts, **Fig. 3C** for representative image, **Fig. F** for quantification) and vimentin (endothelial cells, **Fig. 3D** for representative image, **Fig. 3G** for quantification) revealed a loss of trophoblasts, but not endothelial cells, in placentas from IAV-infected compared with mock-inoculated dams at 3 dpi. Concentrations of IL-13 (**Fig. 3H**), granulocyte-macrophage colony-stimulating factor (GM-CSF, **Fig. 3I**), and IL-18 (**Fig. 3J**), cytokines secreted by trophoblasts *in vitro* (Megli et al., 2021; Naruse et al., 2010), were lower in placentas from IAV-infected than mock-inoculated dams at 3 dpi. By 6 and 8 dpi, neither trophoblast nor endothelial cell numbers differed between placentas of IAV-infected and mock-inoculated dams (**Supplemental Fig. 2**), indicating resolution of placental damage.

3.4 Proinflammatory cytokines peak in the placenta following placental damage during Influenza A virus infection

Proinflammatory cytokines, such as IL-1β and TNFα, in the placenta are associated with placental damage (Chudnovets et al., 2020; Creisher et al., 2022b; Li et al., 2018). Concentrations of proinflammatory cytokines, including IL-1β (**Fig. 4A**), IL-6 (**Fig. 4B**), and TNFα (**Fig. 4C**) exhibited a transient increase in placentas from IAV-infected compared with mock-inoculated dams at 6dpi. The increased concentrations of proinflammatory cytokines followed the placental damage and reductions in trophoblasts observed at 3dpi. The profile of

cytokine secretion in the placenta (**Supplemental Table 3**) differed from the patterns observed in either the spleen (**Supplemental Table 2**) or lungs (**Supplemental Table 1**). Increased secretion of proinflammatory cytokines in the placenta could be mediated by infiltration of immune cells, as we have observed in models of intrauterine inflammation (Liu et al., 2021; Liu et al., 2022). Flow cytometry was used to evaluate adaptive (i.e., B cells, T cells) and innate (i.e., NK cells, neutrophils, eosinophils, macrophages) immune cells in the placenta at 6 dpi (**Fig. 4D-L, Supplemental Fig. 3** for representative gating). Frequencies of $CD45^+$ leukocytes were reduced in placentas of IAV-infected dams compared to mock-inoculated dams (**Fig 4D**), which was further observed for NK cells (**Fig. 4E**), B cells (**Fig. 4F**), $CD4^+$ T cells (**Fig. 4G**), and $CD8^+$ T cells (**Fig. 4H**) in placentas of IAV-infected dams. Frequencies of neutrophils (**Fig. 4I**), eosinophils (**Fig. 4J**) and $CD163^+$ macrophages (**Fig. 4K**) were similar in placentas from IAV- and mock-inoculated dams. $CD68^+$ macrophages were the only immune cell population that exhibited a significant increase in placentas of IAV-infected compared with mock-inoculated dams (**Fig. 4L**). The patterns of immune cell infiltrates observed in placentas were not observed in peripheral blood cells obtained from the same dams (**Supplemental Fig. 4**). $CD68^+$ macrophages in the placenta are associated with intrauterine growth restriction in humans (Berezhna et al., 2021) and secretion of proinflammatory cytokines (Ye et al., 2022). Taken together, these results indicate that maternal respiratory infection with IAV can induce transient but significant cell death and proinflammatory cytokine release at the maternal fetal interface, in the absence of direct viral infection or broad leukocyte infiltration.

3.5 Influenza A virus infection suppresses the pregnancy-associated rise in progesterone via COX-1 activity

The mechanism underlying placental damage and cytokine secretion during IAV infection might involve sex hormone regulation. Placental development and maturation, which occurs at E10-E14 in mice (Hemberger et al., 2020) are supported by P4 signaling in both

humans and mice (Di Renzo et al., 2016; Malassine et al., 2003; Terakawa et al., 2012; Wang et al., 1995). As IAV infection during pregnancy has been associated with reduced circulating P4 in mice (Kim et al., 2012; Littauer et al., 2017; Vermillion et al., 2018), we evaluated if IAV infection of outbred pregnant mice altered circulating (**Fig. 5A**) and placental (**Fig. 5B**) P4 concentrations. Circulating and placental concentrations of P4 in mock-inoculated dams increased throughout gestation and peaked at approximately E16 (**Fig. 5A-B**) (Murr et al., 1974). In contrast, IAV infection significantly reduced circulating and placental P4 concentrations throughout gestation relative to mock-inoculated dams, although not to circulating concentrations observed in nonpregnant females **(Fig. 5A**).

In mice, P4 is secreted by the corpus luteum of the ovary throughout the entire pregnancy where it is canonically regulated by the prostaglandin (PG) F2α (Diaz et al., 2002; Peluso et al., 1980). To evaluate if secreted PGF2α upregulation was associated with reduced P4, PGF2α as well as PGE2, a prostaglandin that has been observed to be upregulated with IAV infection in nonpregnant mice (Coulombe et al., 2014), were measured in the lungs (i.e., the site of IAV replication), systemic circulation, and the ovaries (i.e., the site of P4 secretion) of IAV-infected and mock inoculated dams at 1 and 3 dpi (**Fig. 5C-E**, **Supplemental Fig. 5**). Concentrations of PGF2α, but not PGE2 (**Supplemental Fig.5A-C**), were significantly increased in the lung (**Fig. 5C**), sera (**Fig. 5D**), and ovaries (**Fig. 5E**) of IAV-infected dams as compared with mock-inoculated dams at 3 dpi. Elevated concentrations of PGFα in the ovary were associated with reduced serum P4 in both IAV-infected and mock-inoculated dams (**Supplemental Fig. 5D).**

Prostaglandins, including PGF2α are canonically synthesized by COX enzymes, with COX-1 constitutively expressed in most cells and COX2 induced by inflammatory stimuli (Ricciotti and FitzGerald, 2011). Active COX-1 (Otto et al., 1993), but not COX-2, expression was elevated in the lungs of IAV-infected relative to mock-inoculated dams at 3dpi (**Fig. 5F-G**,

Supplemental Fig. 6). Neither COX-1 nor COX-2 expression were altered in the ovaries (**Supplemental Fig. 7**), suggesting that PGF2α generation by COX-1 is local at the site of IAV infection. To evaluate if COX-1 activity is not just sufficient but necessary for PGF2α secretion and suppression of P4 during IAV-infection, subsets of IAV-infected or mock-inoculated dams at E10 were pretreated with either a COX-1-specific inhibitor (SC560), a COX-2-specific inhibitor (NS-398), or vehicle (**Fig. 5H-I**). COX-1 inhibition, as measured by inhibition of serum thromboxane B2 (TXB2) (Wallace et al., 1998; Wallace et al., 1999), was specific to COX-1 inhibitor treatment and not observed with COX-2 inhibitor treatment (**Supplemental Fig. 8A**). COX-1, but not COX-2, inhibition significantly reduced PGF2α and increased P4 secretion in IAV-infected dams (**Fig. 5H-I**, **Supplemental Fig. 8B**). These data illustrate that IAV infection disrupts activity along the arachidonic acid pathway in pregnant dams to cause suppression of P4, which is required for a healthy pregnancy.

3.6 Synthetic progestin treatment improves IAV-induced maternal morbidity, placental damage, and perinatal developmental delays

To establish whether IAV-infection induced P4 suppression was the cause of adverse maternal and fetal outcomes, a subset of IAV-infected and mock inoculated dams were treated with a single dose of either 17-α-hydroxyprogesterone caproate (17-OHPC), a synthetic progestin that is safe to use during pregnancy (Sibai et al., 2021) or vehicle. The administration of 17-OHPC to mock-inoculated dams had no adverse impact on pregnancy outcomes. Administration of 17-OHPC to IAV-infected dams significantly reduced hypothermia as compared with IAV-infected dams treated with vehicle (**Fig. 6A**). Treatment of IAV-infected dams with 17-OHPC did not affect pulmonary infectious virus titers (**Fig. 6B**). These data suggest that IAV-induced suppression of P4 causes maternal morbidity, independent of controlling virus replication.

To determine if administration of 17-OHPC to IAV-infected dams could reverse adverse perinatal outcomes, subsets of IAV-infected and mock-inoculated dams with and without 17-OHPC treatment carried their pregnancies to term. Treatment of mock-inoculated dams with 17-OHPC had no effect on the development of offspring relative to vehicle-treated, mock-infected dams. In contrast, treatment of IAV-infected dams with 17-OHPC significantly increased birth mass (**Fig. 6C**), mitigated developmental delays in key milestones (**Fig. 6D**), and improved neurobehavioral development as measured by surface righting at PND5 (**Fig. 6E**) as compared with offspring from IAV-infected dams that were treated with vehicle. These data demonstrate that IAV-induced suppression of P4 during pregnancy causes intrauterine growth restriction and postnatal developmental delays, which are reversed by treatment with a safe, synthetic progestin.

We hypothesized that 17-OHPC treatment might prevent placental damage to improve offspring outcomes among IAV-infected dams. Treatment of mock-inoculated dams with 17-OHPC did not alter placental histology, cell death, or numbers of trophoblasts as compared with vehicle-treated, mock-infected dams. In contrast, treatment of IAV-infected dams with 17-OHPC significantly reduced placental cell death (**Fig. 7A-B**), increased proportions of trophoblasts (**Fig. 7C-D**), and reduced placental concentrations of proinflammatory cytokines (**Supplemental Table 4**), including IL-1β (**Fig. 7E**), IL-6 (**Fig. 7F**), and TNFα (**Fig. 7G**). These data illustrate that suppressed P4 is the cause of placental tissue damage and adverse perinatal outcomes during IAV-infection and treatment with 17-OHPC improved maternal, placental, and offspring outcomes during infection.

4 Discussion

Both seasonal and pandemic influenza virus infection during pregnancy result in adverse perinatal and long-term detrimental outcomes that have been reported since the 1918 pandemic (He et al., 2017; Mazumder et al., 2010; Noymer and Garenne, 2000). Using an outbred mouse

model of IAV infection during pregnancy, 2009 H1N1 infection caused maternal morbidity, transient placental damage and inflammation, and long-term offspring growth restriction and developmental delays. The IAV-induced adverse maternal and fetal outcomes were mediated by a COX-1-dependent reduction in P4, including at the maternal-fetal interface. Previous studies report damage to tissue architecture, necrosis, and pro-inflammatory cytokines in the placenta following maternal IAV infection (Antonson et al., 2021; Chan et al., 2010; Van Campen et al., 2020), including associations between placental damage and reduced placental P4 (Littauer et al., 2017; Swieboda et al., 2020). Our study expands upon this literature by establishing a novel causal role for the arachidonic acid biosynthesis pathway, which is activated by IAV infection and disrupts P4 during pregnancy. Our data provide a mechanistic connection between a pulmonary virus infection, which causes elevated COX-1 enzymatic activity, and placental tissue damage, caused by increased prostaglandin (PG) and reduced P4 synthesis. Our results are consistent with knockout studies where selective disruption of progesterone receptor signaling in immune cells causes damage to the placenta, intrauterine growth restriction, and fetal wasting (Severance et al., 2022; Thiele et al., 2019). By treating dams with a synthetic progestin that is safe during pregnancy, the IAV-induced placental damage, inflammation, and adverse fetal outcomes, were reversed, highlighting the translational significance of these findings.

IAV-induced suppression of P4 was dependent on COX-1, but not COX-2, signaling and PGF2α secretion. Progesterone secretion during pregnancy is canonically regulated by PGF2α, which signals in the corpus luteum and induces luteolysis to inhibit P4 secretion (Diaz et al., 2002). PGF2α is generated within the arachidonic acid biosynthesis pathway, where COX enzymes, predominantly COX-1 or COX-2, convert arachidonic acid into prostanoids that are then converted to PG subclasses (i.e., PGF2α) by specific PG synthases (Dubois et al., 1998; Wang et al., 2021). Historically, COX-1 has been characterized as constitutively active and

homeostatic, while COX-2 has been characterized as inducible and associated with pain and inflammation (Adelizzi, 1999; Dubois et al., 1998). COX-1, however, also may have functions in inflammatory responses, as COX-1 inhibition can alleviate neuroinflammation in a mouse model of retinitis pigmentosa (Yang et al., 2020). Further, aspirin given at COX-1-specific doses is associated with reduced rates of preeclampsia (Rolnik et al., 2022). Our data add to this growing body of literature by illustrating that IAV infection upregulates COX-1 in the lungs and increased COX-1-dependent PGF2α in several tissues, including the ovaries.

Mouse models of pregnancy are powerful tools to identify mechanisms of disease pathogenesis and evaluate the safety and efficacy of potential treatments (Vermillion and Klein, 2018); mice, however, have limitations. The full-term gestation for mice is approximately 20 days (about 3 weeks), but 40 weeks (about 9 months) for humans, with disproportionally more gestational time spent in the first-trimester equivalent in mice than in humans (Sones and Davisson, 2016). Further, placental anatomy differs between mice and humans [reviewed in (Ander et al., 2019)], with, for example, the placental labyrinth structure found in mice but not humans. Inbred mice further lack genetic heterogeneity at the maternal-fetal interface, and in the current study, outbred mice were used to avoid this limitation (Reichenbach et al., 2013). With the use of outbred mice, genetic manipulations were not available to test hypotheses; instead, pharmacologic inhibitors were used, which could have off-target effects, despite dosages optimized for target-specificity.

Despite these limitations, results from this study highlight the value of treatments that mitigate disease in addition to antiviral treatments for influenza during pregnancy. In the current study, we utilized 17-OHPC, a synthetic progestin that has been prescribed to pregnant women with history of preterm birth (EPPPIC Group, 2021). While the US FDA has withdrawn approval due to a lack of efficacy of 17-OHPC for preterm birth (U.S. Food & Drug Administration, 2023), translational studies demonstrated that progesterone and 17-OHPC, specifically, may contribute

to maternal immunomodulation and prevention of adverse perinatal outcomes other than preterm birth (Novak et al., 2018; Severance et al., 2022). Furthermore, while nonselective COX inhibitors [i.e. non-steroidal anti-inflammatory drugs (NSAIDs)] are generally not recommend for use during pregnancy (Ostensen and Skomsvoll, 2004; U.S. Food & Drug Administration, 2022), we have identified COX-1-dependent P4 regulation as a targetable pathway that warrants further investigation. Our results add to growing literature utilizing P4 to treat adverse pregnancy and perinatal outcomes (Alawadhi et al., 2022; Novak et al., 2018; Pei et al., 2022; Severance et al., 2022). With pregnant people considered an 'at risk' population for many infectious diseases ranging from influenza viruses and SARS-CoV-2 to Zika viruses, greater consideration should be given to identifying the mechanisms of adverse pregnancy outcomes and the off label use of compounds (e.g., 17-OHPC) that are safe during pregnancy and could mitigate the impact of infectious diseases at the maternal-fetal interface.

5 Acknowledgements

The authors would like to thank the Klein, Pekosz, Davis, and Baumgarth laboratories for discussions about these data. We would also like to thank the expert animal care staff at the Johns Hopkins School of Public Health for assistance with maintenance of pregnant dams.

6 Funding

Funding provided by NIH/NICHD R01HD097608 (I.B. and S.L.K), the NIH/ORWH/NIA Specialized Center of Research Excellence in Sex Differences U54AG062333 (S.L.K), NIH/NIAID training grant T32AI007417-26 (P.C. and M.S.), the Vivien Thomas Scholars Initiative at the Johns Hopkins University (A.C.).

7 Contributions

SK, PC, MP, and IB conceptualized and designed the experiments. PC, MP, JP, AC, and MS performed animal experiments. PC grew and quantified viruses and multiplexed cytokines. PC and MP performed ELISA and Western blot. PC, JP, and JinL performed flow cytometry. JunL

stained, imaged, and analyzed placental tissue. PC statistically analyzed and graphed data. PC and SK wrote the manuscript with input from all authors. All authors read and provided edits to drafts and approved the final submission. The order of authors was determined based on contributions to the overall design, experimentation, analyses, and writing.

8 References

Abu-Raya, B., C. Michalski, M. Sadarangani, and P.M. Lavoie. 2020. Maternal Immunological Adaptation During Normal Pregnancy. *Front Immunol* 11:575197.

Adelizzi, R.A. 1999. COX-1 and COX-2 in health and disease. *J Am Osteopath Assoc* 99:S7-12.

Alawadhi, M., A. Mouihate, N. Kilarkaje, and M. Al-Bader. 2022. Progesterone partially recovers placental glucose transporters in dexamethasone-induced intrauterine growth restriction. *Reprod Biomed Online* 44:595-607.

Ander, S.E., M.S. Diamond, and C.B. Coyne. 2019. Immune responses at the maternal-fetal interface. *Sci Immunol* 4:

Antonson, A.M., A.D. Kenney, H.J. Chen, K.N. Corps, J.S. Yount, and T.L. Gur. 2021. Moderately pathogenic maternal influenza A virus infection disrupts placental integrity but spares the fetal brain. *Brain Behav Immun* 96:28-39.

Arany, Z., D. Hilfiker-Kleiner, and S.A. Karumanchi. 2022. Animal Models of Cardiovascular Complications of Pregnancy. *Circ Res* 130:1763-1779.

Berezhna, V.A., T.V. Mamontova, and A.M. Gromova. 2021. Cd68+ M1 Macrophages Is Associated with Placental Insufficiency under Fetal Growth Restriction. *Wiad Lek* 74:213-219.

Brown, A.S., M.D. Begg, S. Gravenstein, C.A. Schaefer, R.J. Wyatt, M. Bresnahan, V.P. Babulas, and E.S. Susser. 2004. Serologic evidence of prenatal influenza in the etiology of schizophrenia. *Arch Gen Psychiatry* 61:774-780.

Chan, K.H., A.J. Zhang, K.K. To, C.C. Chan, V.K. Poon, K. Guo, F. Ng, Q.W. Zhang, V.H. Leung, A.N. Cheung, C.C. Lau, P.C. Woo, H. Tse, W. Wu, H. Chen, B.J. Zheng, and K.Y. Yuen. 2010. Wild type and mutant 2009 pandemic influenza A (H1N1) viruses cause more severe disease and higher mortality in pregnant BALB/c mice. *PLoS One* 5:e13757.

Chudnovets, A., J. Lei, Q. Na, J. Dong, H. Narasimhan, S.L. Klein, and I. Burd. 2020. Dose-dependent structural and immunological changes in the placenta and fetal brain in response to systemic inflammation during pregnancy. *Am J Reprod Immunol* 84:e13248.

Coulombe, F., J. Jaworska, M. Verway, F. Tzelepis, A. Massoud, J. Gillard, G. Wong, G. Kobinger, Z. Xing, C. Couture, P. Joubert, J.H. Fritz, W.S. Powell, and M. Divangahi. 2014. Targeted prostaglandin E2 inhibition enhances antiviral immunity through induction of type I interferon and apoptosis in macrophages. *Immunity* 40:554-568.

Cox, S., S.F. Posner, M. McPheeters, D.J. Jamieson, A.P. Kourtis, and S. Meikle. 2006. Influenza and pregnant women: hospitalization burden, United States, 1998-2002. *J Womens Health (Larchmt)* 15:891-893.

Creisher, P.S., A.D. Campbell, J.L. Perry, K. Roznik, I. Burd, and S.L. Klein. 2022a. Influenza subtype-specific maternal antibodies protect offspring against infection but inhibit vaccine-induced immunity and protection in mice. *Vaccine* 40:6818-6829.

Creisher, P.S., J. Lei, M.L. Sherer, A. Dziedzic, A.E. Jedlicka, H. Narasimhan, A. Chudnovets, A.D. Campbell, A. Liu, A. Pekosz, I. Burd, and S.L. Klein. 2022b. Downregulation of transcriptional activity, increased inflammation, and damage in the placenta following in utero Zika virus infection is associated with adverse pregnancy outcomes. *Front Virol* 2:

Creisher, P.S., J.L. Perry, W. Zhong, J. Lei, K.R. Mulka, W.H. Ryan, R. Zhou, E.H. Akin, A. Liu, W. Mitzner, I. Burd, A. Pekosz, and S.L. Klein. 2023. Adverse outcomes in SARS-CoV-2 infected pregnant mice are gestational age-dependent and resolve with antiviral treatment. *The Journal of Clinical Investigation*

Di Renzo, G.C., I. Giardina, G. Clerici, E. Brillo, and S. Gerli. 2016. Progesterone in normal and pathological pregnancy. *Horm Mol Biol Clin Investig* 27:35-48.

Diaz, F.J., L.E. Anderson, Y.L. Wu, A. Rabot, S.J. Tsai, and M.C. Wiltbank. 2002. Regulation of progesterone and prostaglandin F2alpha production in the CL. *Mol Cell Endocrinol* 191:65-80.

Dubois, R.N., S.B. Abramson, L. Crofford, R.A. Gupta, L.S. Simon, L.B. Van De Putte, and P.E. Lipsky. 1998. Cyclooxygenase in biology and disease. *FASEB J* 12:1063-1073.

Elovitz, M.A., Z. Wang, E.K. Chien, D.F. Rychlik, and M. Phillippe. 2003. A new model for inflammation-induced preterm birth: the role of platelet-activating factor and Toll-like receptor-4. *Am J Pathol* 163:2103-2111.

Engels, G., A.M. Hierweger, J. Hoffmann, R. Thieme, S. Thiele, S. Bertram, C. Dreier, P. Resa-Infante, H. Jacobsen, K. Thiele, M. Alawi, D. Indenbirken, A. Grundhoff, S. Siebels, N. Fischer, V. Stojanovska, D. Muzzio, F. Jensen, K. Karimi, H.W. Mittrucker, P.C. Arck, and G. Gabriel. 2017. Pregnancy-Related Immune Adaptation Promotes the Emergence of Highly Virulent H1N1 Influenza Virus Strains in Allogenically Pregnant Mice. *Cell Host Microbe* 21:321-333.

EPPPIC Group. 2021. Evaluating Progestogens for Preventing Preterm birth International Collaborative (EPPPIC): meta-analysis of individual participant data from randomised controlled trials. *Lancet* 397:1183-1194.

Feather-Schussler, D.N., and T.S. Ferguson. 2016. A Battery of Motor Tests in a Neonatal Mouse Model of Cerebral Palsy. *J Vis Exp*

Futaki, N., K. Yoshikawa, Y. Hamasaka, I. Arai, S. Higuchi, H. Iizuka, and S. Otomo. 1993. NS-398, a novel non-steroidal anti-inflammatory drug with potent analgesic and antipyretic effects, which causes minimal stomach lesions. *Gen Pharmacol* 24:105-110.

Hall, O.J., R. Nachbagauer, M.S. Vermillion, A.L. Fink, V. Phuong, F. Krammer, and S.L. Klein. 2017. Progesterone-Based Contraceptives Reduce Adaptive Immune Responses and Protection against Sequential Influenza A Virus Infections. *J Virol* 91:

Hartel, C., A. Humberg, D. Viemann, A. Stein, T. Orlikowsky, J. Rupp, M.V. Kopp, E. Herting, and W. Gopel. 2016. Preterm Birth during Influenza Season Is Associated with Adverse Outcome in Very Low Birth Weight Infants. *Front Pediatr* 4:130.

He, J., Z.W. Liu, Y.P. Lu, T.Y. Li, X.J. Liang, P.C. Arck, S.M. Huang, B. Hocher, and Y.P. Chen. 2017. A Systematic Review and Meta-Analysis of Influenza A Virus Infection During Pregnancy

Associated with an Increased Risk for Stillbirth and Low Birth Weight. *Kidney Blood Press Res* 42:232-243.

Hemberger, M., C.W. Hanna, and W. Dean. 2020. Mechanisms of early placental development in mouse and humans. *Nat Rev Genet* 21:27-43.

Heyser, C.J. 2004. Assessment of developmental milestones in rodents. *Curr Protoc Neurosci* Chapter 8:Unit 8 18.

Hill, J.M., M.A. Lim, and M.M. Stone. 2008. Developmental Milestones in the Newborn Mouse. In Neuropeptide Techniques. I. Gozes, editor Humana Press, Totowa, NJ. 131-149.

Jacobsen, H., K. Walendy-Gnirss, N. Tekin-Bubenheim, N.M. Kouassi, I. Ben-Batalla, N. Berenbrok, M. Wolff, V.P. Dos Reis, M. Zickler, L. Scholl, A. Gries, H. Jania, A. Kloetgen, A. Dusedau, G. Pilnitz-Stolze, A. Jeridi, A.O. Yildirim, H. Fuchs, V. Gailus-Durner, C. Stoeger, M.H. de Angelis, T. Manuylova, K. Klingel, F.J. Culley, J. Behrends, S. Loges, B. Schneider, S. Krauss-Etschmann, P. Openshaw, and G. Gabriel. 2021. Offspring born to influenza A virus infected pregnant mice have increased susceptibility to viral and bacterial infections in early life. *Nat Commun* 12:4957.

Kanmaz, H.G., O. Erdeve, S.S. Ogz, N. Uras, S. Celen, G. Korukluoglu, S. Zergeroglu, A. Kara, and U. Dilmen. 2011. Placental transmission of novel pandemic influenza a virus. *Fetal Pediatr Pathol* 30:280-285.

Katz, M.A., B.D. Gessner, J. Johnson, B. Skidmore, M. Knight, N. Bhat, H. Marshall, D.J. Horne, J.R. Ortiz, and D.B. Fell. 2017. Incidence of influenza virus infection among pregnant women: a systematic review. *BMC Pregnancy Childbirth* 17:155.

Kim, H.M., Y.M. Kang, B.M. Song, H.S. Kim, and S.H. Seo. 2012. The 2009 pandemic H1N1 influenza virus is more pathogenic in pregnant mice than seasonal H1N1 influenza virus. *Viral Immunol* 25:402-410.

Klein, S.L., C. Passaretti, M. Anker, P. Olukoya, and A. Pekosz. 2010. The impact of sex, gender and pregnancy on 2009 H1N1 disease. *Biol Sex Differ* 1:5.

Krishnan, L., T. Nguyen, and S. McComb. 2013. From mice to women: the conundrum of immunity to infection during pregnancy. *J Reprod Immunol* 97:62-73.

Lauzon-Joset, J.F., N.M. Scott, K.T. Mincham, P.A. Stumbles, P.G. Holt, and D.H. Strickland. 2019. Pregnancy Induces a Steady-State Shift in Alveolar Macrophage M1/M2 Phenotype That Is Associated With a Heightened Severity of Influenza Virus Infection: Mechanistic Insight Using Mouse Models. *J Infect Dis* 219:1823-1831.

Li, Z.H., L.L. Wang, H. Liu, K.P. Muyayalo, X.B. Huang, G. Mor, and A.H. Liao. 2018. Galectin-9 Alleviates LPS-Induced Preeclampsia-Like Impairment in Rats via Switching Decidual Macrophage Polarization to M2 Subtype. *Front Immunol* 9:3142.

Littauer, E.Q., E.S. Esser, O.Q. Antao, E.V. Vassilieva, R.W. Compans, and I. Skountzou. 2017. H1N1 influenza virus infection results in adverse pregnancy outcomes by disrupting tissue-specific hormonal regulation. *PLoS Pathog* 13:e1006757.

Liu, J., Y. Liu, S. Panda, A. Liu, J. Lei, and I. Burd. 2021. Type 1 Cytotoxic T Cells Increase in Placenta after Intrauterine Inflammation. *Front Immunol* 12:718563.

Liu, Y., Q. Na, J. Liu, A. Liu, A. Oppong, J.Y. Lee, A. Chudnovets, J. Lei, R. Sharma, S. Kannan, R.M. Kannan, and I. Burd. 2022. Dendrimer-Based N-Acetyl Cysteine Maternal Therapy

682 Ameliorates Placental Inflammation via Maintenance of M1/M2 Macrophage
683 Recruitment. *Front Bioeng Biotechnol* 10:819593.
684 Malassine, A., J.L. Frendo, and D. Evain-Brion. 2003. A comparison of placental development
685 and endocrine functions between the human and mouse model. *Hum Reprod Update*
686 9:531-539.
687 Marcelin, G., J.R. Aldridge, S. Duan, H.E. Ghoneim, J. Rehg, H. Marjuki, A.C. Boon, J.A. McCullers,
688 and R.J. Webby. 2011. Fatal outcome of pandemic H1N1 2009 influenza virus infection is
689 associated with immunopathology and impaired lung repair, not enhanced viral burden,
690 in pregnant mice. *J Virol* 85:11208-11219.
691 Mazumder, B., D. Almond, K. Park, E.M. Crimmins, and C.E. Finch. 2010. Lingering prenatal
692 effects of the 1918 influenza pandemic on cardiovascular disease. *J Dev Orig Health Dis*
693 1:26-34.
694 Megli, C., S. Morosky, D. Rajasundaram, and C.B. Coyne. 2021. Inflammasome signaling in
695 human placental trophoblasts regulates immune defense against Listeria
696 monocytogenes infection. *J Exp Med* 218:
697 Meijer, W.J., A.M. Wensing, H.W. Bruinse, and P.G. Nikkels. 2014. High rate of chronic villitis in
698 placentas of pregnancies complicated by influenza A/H1N1 infection. *Infect Dis Obstet*
699 *Gynecol* 2014:768380.
700 Mertz, D., J. Geraci, J. Winkup, B.D. Gessner, J.R. Ortiz, and M. Loeb. 2017. Pregnancy as a risk
701 factor for severe outcomes from influenza virus infection: A systematic review and
702 meta-analysis of observational studies. *Vaccine* 35:521-528.
703 Moldenhauer, L.M., J.D. Hayball, and S.A. Robertson. 2010. Utilising T cell receptor transgenic
704 mice to define mechanisms of maternal T cell tolerance in pregnancy. *J Reprod Immunol*
705 87:1-13.
706 Murr, S.M., G.H. Stabenfeldt, G.E. Bradford, and Geschwind, II. 1974. Plasma progesterone
707 during pregnancy in the mouse. *Endocrinology* 94:1209-1211.
708 Naruse, K., B.A. Innes, J.N. Bulmer, S.C. Robson, R.F. Searle, and G.E. Lash. 2010. Secretion of
709 cytokines by villous cytotrophoblast and extravillous trophoblast in the first trimester of
710 human pregnancy. *J Reprod Immunol* 86:148-150.
711 Neuzil, K.M., G.W. Reed, E.F. Mitchel, L. Simonsen, and M.R. Griffin. 1998. Impact of influenza
712 on acute cardiopulmonary hospitalizations in pregnant women. *Am J Epidemiol*
713 148:1094-1102.
714 Novak, C.M., M. Ozen, M. McLane, S. Alqutub, J.Y. Lee, J. Lei, and I. Burd. 2018. Progesterone
715 improves perinatal neuromotor outcomes in a mouse model of intrauterine
716 inflammation via immunomodulation of the placenta. *Am J Reprod Immunol* 79:e12842.
717 Noymer, A., and M. Garenne. 2000. The 1918 influenza epidemic's effects on sex differentials in
718 mortality in the United States. *Popul Dev Rev* 26:565-581.
719 Omer, S.B., R. Bednarczyk, S.A. Madhi, and K.P. Klugman. 2012. Benefits to mother and child of
720 influenza vaccination during pregnancy. *Hum Vaccin Immunother* 8:130-137.
721 Omer, S.B., D. Goodman, M.C. Steinhoff, R. Rochat, K.P. Klugman, B.J. Stoll, and U.
722 Ramakrishnan. 2011. Maternal influenza immunization and reduced likelihood of
723 prematurity and small for gestational age births: a retrospective cohort study. *PLoS Med*
724 8:e1000441.

Ostensen, M.E., and J.F. Skomsvoll. 2004. Anti-inflammatory pharmacotherapy during pregnancy. *Expert Opin Pharmacother* 5:571-580.

Otto, J.C., D.L. DeWitt, and W.L. Smith. 1993. N-glycosylation of prostaglandin endoperoxide synthases-1 and -2 and their orientations in the endoplasmic reticulum. *J Biol Chem* 268:18234-18242.

Parboosing, R., Y. Bao, L. Shen, C.A. Schaefer, and A.S. Brown. 2013. Gestational influenza and bipolar disorder in adult offspring. *JAMA Psychiatry* 70:677-685.

Pazos, M.A., T.A. Kraus, C. Munoz-Fontela, and T.M. Moran. 2012. Estrogen mediates innate and adaptive immune alterations to influenza infection in pregnant mice. *PLoS One* 7:e40502.

Pei, J., Z. Liu, C. Wang, N. Chu, L. Liu, Y. Tang, H. Liu, Q. Xiang, H. Cheng, M. Li, and W. Gu. 2022. Progesterone Attenuates SIRT1-Deficiency-Mediated Pre-Eclampsia. *Biomolecules* 12:

Peluso, J.J., S. Leiper, and R.W. Steger. 1980. Effects of PGF2 alpha-induced luteolysis and progesterone on follicular growth in pregnant mice. *Prostaglandins* 19:437-447.

Reichenbach, D.K., Q. Li, R.A. Hoffman, A.L. Williams, W.D. Shlomchik, D.M. Rothstein, A.J. Demetris, and F.G. Lakkis. 2013. Allograft outcomes in outbred mice. *Am J Transplant* 13:580-588.

Ricciotti, E., and G.A. FitzGerald. 2011. Prostaglandins and inflammation. *Arterioscler Thromb Vasc Biol* 31:986-1000.

Rolnik, D.L., K.H. Nicolaides, and L.C. Poon. 2022. Prevention of preeclampsia with aspirin. *Am J Obstet Gynecol* 226:S1108-S1119.

Severance, A.L., J.M. Kinder, L. Xin, A.R. Burg, T.Y. Shao, G. Pham, T. Tilburgs, W.A. Goodman, S. Mesiano, and S.S. Way. 2022. Maternal-fetal conflict averted by progesterone- induced FOXP3+ regulatory T cells. *iScience* 25:104400.

Shaik, I.H., J.R. Bastian, Y. Zhao, S.N. Caritis, and R. Venkataramanan. 2016. Route of administration and formulation dependent pharmacokinetics of 17-hydroxyprogesterone caproate in rats. *Xenobiotica* 46:169-174.

Sibai, B., G.R. Saade, A.F. Das, and J. Gudeman. 2021. Safety review of hydroxyprogesterone caproate in women with a history of spontaneous preterm birth. *J Perinatol* 41:718-725.

Sones, J.L., and R.L. Davisson. 2016. Preeclampsia, of mice and women. *Physiol Genomics* 48:565-572.

Song, J.Y., K.V. Park, S.W. Han, M.J. Choi, J.Y. Noh, H.J. Cheong, W.J. Kim, M.J. Oh, and G.J. Cho. 2020. Paradoxical long-term impact of maternal influenza infection on neonates and infants. *BMC Infect Dis* 20:502.

Swieboda, D., E.Q. Littauer, J.T. Beaver, L.K. Mills, K.M. Bricker, E.S. Esser, O.Q. Antao, D.T. Williams, and I. Skountzou. 2020. Pregnancy Downregulates Plasmablast Metabolic Gene Expression Following Influenza Without Altering Long-Term Antibody Function. *Front Immunol* 11:1785.

Tafuri, A., J. Alferink, P. Moller, G.J. Hammerling, and B. Arnold. 1995. T cell awareness of paternal alloantigens during pregnancy. *Science* 270:630-633.

Tanigawa, T., T. Watanabe, M. Hamaguchi, E. Sasaki, K. Tominaga, Y. Fujiwara, N. Oshitani, T. Matsumoto, K. Higuchi, and T. Arakawa. 2004. Anti-inflammatory effect of two isoforms

767 of COX in H. pylori-induced gastritis in mice: possible involvement of PGE2. *Am J Physiol*
768 *Gastrointest Liver Physiol* 286:G148-156.
769 Teijaro, J.R. 2015. The role of cytokine responses during influenza virus pathogenesis and
770 potential therapeutic options. *Curr Top Microbiol Immunol* 386:3-22.
771 Terakawa, J., T. Watanabe, R. Obara, M. Sugiyama, N. Inoue, Y. Ohmori, Y.Z. Hosaka, and E.
772 Hondo. 2012. The complete control of murine pregnancy from embryo implantation to
773 parturition. *Reproduction* 143:411-415.
774 Thiele, K., A.M. Hierweger, J.I.A. Riquelme, M.E. Solano, J.P. Lydon, and P.C. Arck. 2019.
775 Impaired Progesterone-Responsiveness of CD11c(+) Dendritic Cells Affects the
776 Generation of CD4(+) Regulatory T Cells and Is Associated With Intrauterine Growth
777 Restriction in Mice. *Front Endocrinol (Lausanne)* 10:96.
778 Thomas, D.M., and D.M. Kuhn. 2005. Cyclooxygenase-2 is an obligatory factor in
779 methamphetamine-induced neurotoxicity. *J Pharmacol Exp Ther* 313:870-876.
780 U.S. Food & Drug Administration. 2022. FDA recommends avoiding use of NSAIDs in pregnancy
781 at 20 weeks or later because they can result in low amniotic fluid. In.
782 U.S. Food & Drug Administration. 2023. FDA Commissioner and Chief Scientist Announce
783 Decision to Withdraw Approval of Makena. In.
784 Van Campen, H., J.V. Bishop, V.M. Abrahams, H. Bielefeldt-Ohmann, C.K. Mathiason, G.J.
785 Bouma, Q.A. Winger, C.E. Mayo, R.A. Bowen, and T.R. Hansen. 2020. Maternal Influenza
786 A Virus Infection Restricts Fetal and Placental Growth and Adversely Affects the Fetal
787 Thymic Transcriptome. *Viruses* 12:
788 Vermillion, M.S., and S.L. Klein. 2018. Pregnancy and infection: using disease pathogenesis to
789 inform vaccine strategy. *NPJ Vaccines* 3:6.
790 Vermillion, M.S., A. Nelson, L. Vom Steeg, J. Loube, W. Mitzner, and S.L. Klein. 2018. Pregnancy
791 preserves pulmonary function following influenza virus infection in C57BL/6 mice. *Am J*
792 *Physiol Lung Cell Mol Physiol* 315:L517-L525.
793 Versteeg, L., X. Le Guezennec, B. Zhan, Z. Liu, M. Angagaw, J.D. Woodhouse, S. Biswas, and C.M.
794 Beaumier. 2017. Transferring Luminex(R) cytokine assays to a wall-less plate technology:
795 Validation and comparison study with plasma and cell culture supernatants. *J Immunol*
796 *Methods* 440:74-82.
797 Vousden, N., K. Bunch, M. Knight, and U.I.C.-I. Group. 2021. Incidence, risk factors and impact
798 of seasonal influenza in pregnancy: A national cohort study. *PLoS One* 16:e0244986.
799 Wallace, J.L., A. Bak, W. McKnight, S. Asfaha, K.A. Sharkey, and W.K. MacNaughton. 1998.
800 Cyclooxygenase 1 contributes to inflammatory responses in rats and mice: implications
801 for gastrointestinal toxicity. *Gastroenterology* 115:101-109.
802 Wallace, J.L., K. Chapman, and W. McKnight. 1999. Limited anti-inflammatory efficacy of cyclo-
803 oxygenase-2 inhibition in carrageenan-airpouch inflammation. *Br J Pharmacol* 126:1200-
804 1204.
805 Wang, B., L. Wu, J. Chen, L. Dong, C. Chen, Z. Wen, J. Hu, I. Fleming, and D.W. Wang. 2021.
806 Metabolism pathways of arachidonic acids: mechanisms and potential therapeutic
807 targets. *Signal Transduct Target Ther* 6:94.

Wang, M.W., D.L. Crombie, J.S. Hayes, and R.B. Heap. 1995. Aberrant maternal behaviour in mice treated with a progesterone receptor antagonist during pregnancy. *J Endocrinol* 145:371-377.

Woolston, W.J., and D.O. Conley. 1918. Epidemic Pneumonia (Spanish Influenza) in Pregnancy: Effect in One Hundred and One Cases. *Journal of the American Medical Association* 71:1898-1899.

Yang, W., G. Xiong, and B. Lin. 2020. Cyclooxygenase-1 mediates neuroinflammation and neurotoxicity in a mouse model of retinitis pigmentosa. *J Neuroinflammation* 17:306.

Ye, J., E.M. Sorrell, Y. Cai, H. Shao, K. Xu, L. Pena, D. Hickman, H. Song, M. Angel, R.A. Medina, B. Manicassamy, A. Garcia-Sastre, and D.R. Perez. 2010. Variations in the hemagglutinin of the 2009 H1N1 pandemic virus: potential for strains with altered virulence phenotype? *PLoS Pathog* 6:e1001145.

Ye, Y., L. Peng, A. Chelariu-Raicu, C. Kuhn, X. Dong, U. Jeschke, and V. von Schonfeldt. 2022. Prostaglandin E2 receptor 3 promotes M1 macrophages polarization in unexplained recurrent pregnancy loss. *Biol Reprod* 106:910-918.

Figure Legends

Figure 1. Influenza A virus infection of pregnant outbred mice results in morbidity and a pulmonary cytokine storm.

Dams at embryonic day (E) 10 were intranasally inoculated with 10^3 $TCID_{50}$ of 2009 H1N1 or were mock inoculated with media. Daily maternal body mass (A) and rectal temperature (B) were recorded as measures of maternal morbidity for 14 days. Subsets of dams were euthanized to measure viral titers in lung tissue via $TCID_{50}$ assay (C) and cytokine concentrations in spleen and lung tissue (D) at 3 (E13), 6 (E16), and 8 (E18) days post infection. Individual symbols (A-B) or bars (C) represent the mean ± standard error of the mean from two independent replications (n =12-13/group) with individual mice indicated by symbols (C). Significant differences ($p < 0.05$) were determined by two tailed unpaired t-test of AUCs (A-B) or one-way ANOVA with Bonferroni post hoc test (C) and are indicated by an asterisk (*).

Figure 2. Influenza A virus (IAV) infection during pregnancy causes offspring growth restriction and developmental delays.

Dams at embryonic day (E) 10 were intranasally inoculated with 10^3 $TCID_{50}$ of 2009 H1N1 or were mock inoculated with media and were followed through delivery. Offspring were followed through postnatal day (PND) 21 to assess fetal outcomes. Litter size (A), mass (B), nose to anus length (C), and ear to head diameter (D) were measured at PND 0. Average measurements of each independent litter were graphed to account for litter effects. Average pup mass for each litter was taken daily to track growth through PND 21 (E). Developmental milestones including fur growth, ear canal opening, eye opening, and teeth eruption were recorded (F). At PND 5, a subset of pups was sexed and assessed for their surface righting ability to measure neurological development. One pup per sex per dam was given 3 trials given for the test, and each pup's best trial was reported (G). Bars (A-D, G) represent the mean ± standard error of the mean from two independent replications (n =13/group) with individual litters (A-D) or mice (G) indicated by symbols. For developmental milestones, the center bar indicates the median day a litter reached each milestone, with the range indicated by the edges of the box (D). Significant differences ($p < 0.05$) were determined by two tailed unpaired t-test (A-D), two tailed unpaired t-test of AUCs (E), Mann-Whitney nonparametric test (F), or two-way ANOVA with Bonferroni post hoc test (G) and are indicated by an asterisk (*).

Figure 3. Influenza A virus infection during pregnancy causes placental damage and disruption to the trophoblast-endothelial cell barrier.

Dams at embryonic day (E) 10 were intranasally inoculated with 10^3 $TCID_{50}$ of 2009 H1N1 or were mock inoculated with media and were euthanized at 3 dpi (E13) to collect placentas. Representative H&E images were taken at 5x magnification and 20x magnification with arrows indicating red blood cells (A). Representative $TUNEL^+$ (green) stained placentas with DAPI to label nuclei taken (blue) were taken at 20x magnification and 100x (B). Placentas were immunostained for cytokeratin (C, red) to mark trophoblasts or vimentin (D, red) to mark endothelial cells and DAPI (blue) to label nuclei. Representative images were taken at

20x magnification and further zoomed 2.90-fold. Quantification of the percentage positive area for each marker is shown (E-G). Placentas were homogenized and analyzed for concentrations (pg/ml) of IL-13 (H), GM-CSF (I), and IL-18 (J). Bars represent the mean ± standard error of the mean [n =5-6/group (image quantification) and 11-14/group (cytokines)] with each symbol indicating one placenta and, for analysis of images, is the mean quantification of 6 fields of view. Significant differences ($p < 0.05$) were determined by unpaired two tailed t-test and are indicated by an asterisk (*). Scale bar: 1 mm (A, left panel/group), 100 µm [(A, right panels/group; B, left panel/group), 200 µm (C-D, left panel/group), or 50 µm (C-D, right panel/group).

Figure 4. Placental concentrations of proinflammatory cytokines and immune cells peak at 6 days-post infection.

Dams at embryonic day 10 were intranasally inoculated with 10^3 $TCID_{50}$ of 2009 H1N1 or were mock inoculated with media and were euthanized at 3 (E13), 6 (E16), or 8 dpi (E18) to collect placental tissue (A-C). Placentas were homogenized and analyzed for concentrations (pg/ml) of proinflammatory cytokines, including IL-1β (A), IL-6 (B), and TNFα (C). Flow cytometry was performed using live placental cells at 6 dpi to assess immune cell type frequencies in placental tissue including leukocytes ($CD45^+$, D), NK cells ($CD45^+$, $CD3^-$,$CD19^+$, E), B cells ($CD45^+$, $CD3^-$,$CD19^+$, F), $CD4^+$ T-cells ($CD45^+$, $CD3^+$, $CD4^+$, G), $CD8^+$ T cells ($CD45^+$, $CD3^+$, $CD8a^+$, H), neutrophils ($CD45^+$, $CD11b^+$, $F4/80^-$, $CD170^-$, side scatter area high, I), eosinophils ($CD45^+$, $CD11b^+$, $F4/80^+$, $CD170^+$, J), $CD163^+$ macrophages ($CD45^+$, $CD11b^+$, $F4/80^+$, $CD163^+$, K), and CD68+ macrophages ($CD45^+$, $CD11b^+$, $F4/80^+$, $CD68^+$, L). Bars represent the mean ± standard error of the mean from two independent replications (n =11-14/group for cytokines and 5/group for flow cytometry) with individual mice indicated by symbols. Significant differences ($p < 0.05$) were determined by two-way ANOVA with Bonferroni post hoc test (A-C) or two tailed unpaired t-test (D-L) and are indicated by an asterisk (*).

Figure 5. Downregulation of circulating and placental P4 caused by upregulation of COX-1 through PGF2α secretion. Dams at embryonic day (E) 10 were intranasally inoculated with 10^3 $TCID_{50}$ of 2009 H1N1 or were mock inoculated with media. Dams were euthanized for tissue and serum collection at 1 (E11), 3 (E13), 6 (E16) or 8 (E18) dpi. Serum (A) and placental (B) P4 concentrations (ng.ml) were measured by ELISA. PGF2α concentrations (ng/ml) were measured by ELISA in lung homogenates (C), serum (D), and ovarian homogenates (E). COX-1 and COX-2 protein expression in lung tissue was assessed by western blot at 3dpi (F) and quantified as the fluorescence signal for each protein normalized to GAPDH. Active COX-1 is also shown as a ratio to inactive COX-1 (F). Lungs from two independent experiments were analyzed together to minimize interassay variability. Independent cohorts of dams were intranasally inoculated with 10^3 $TCID_{50}$ of 2009 H1N1 or were mock inoculated with media and treated twice daily beginning 1 day before infection with either COX-1 inhibitor (SC-560, 10 mg/kg), COX-2 inhibitor (NS-398, 10 mg/kg), or vehicle until dams were euthanized at 3 dpi for tissue and serum collection. PGF2α concentrations (ng/ml) were measured by ELISA in ovarian tissue (H) and P4 concentrations (ng/ml) were measured by ELISA in serum (I). Bars represent the mean ± standard error of the mean from two independent replications (n =6-12/group for ELISAs and 4/group for western blot) with individual mice indicated by symbols. Significant differences ($p < 0.05$) were determined by two-way ANOVA with Bonferroni post hoc test (A-E, H-I) or two tailed unpaired t-test (G) and are indicated by an asterisk (*).

Figure 6. Synthetic progestin treatment improves maternal morbidity and prevents offspring growth restriction and developmental delays.

Dams at embryonic day (E) 10 were intranasally inoculated with 10^3 $TCID_{50}$ of 2009 H1N1 or were mock inoculated with media. At the time of inoculation, dams were subcutaneously administered 17α-hydroxyprogesterone caproate (17-OHPC, 2mg/dam). Dams were euthanized

for tissue collection at 3 (E13) or 6 (E16) days post infection (dpi) or carried their pregnancy through delivery (E20). Daily rectal temperatures were recorded as a measurement of maternal morbidity through 14dpi (A). Viral titers were measured in lung tissue via $TCID_{50}$ assay at 3 (E13) and 6 (E16) dpi (B). At postnatal day (PND) 0, pups were weighed, with the average measurements of each independent litter graphed to account for litter effects (C), and pups were followed through weaning to observe developmental milestones (D) including fur growth, ear canal opening, eye opening, and teeth eruption. (E) At PND 5, a subset of pups was sexed and assessed for their surface righting ability with one pup per sex per dam given 3 trials for the test, and each pup's best trial reported (G). Individual symbols (A) or bars (B-C, E) represent the mean ± standard error of the mean from two independent replications (n =10/group) with individual mice (B, E) or litters (C) indicated by symbols. For developmental milestones, the center bar indicates the median day a littler reached each milestone, with the range indicated by the edges of the box (D). Significant differences ($p < 0.05$) were determined by two-way ANOVA with Bonferroni post hoc test of AUCs (A), two-way ANOVA with Bonferroni post hoc test (B-C), Kruskal-Wallis with Dun's post hoc test (D), or three-way ANOVA with Bonferroni post hoc test (G) and are indicated by an asterisk (*).

Figure 7. Synthetic progestin treatment ameliorates placental damage and inflammation. Dams at embryonic day (E) 10 were intranasally inoculated with 10^3 $TCID_{50}$ of 2009 H1N1 or were mock inoculated with media. At the time of inoculation, dams were subcutaneously administered 17α-hydroxyprogesterone caproate (17-OHPC, 2mg/dam). Placentas were collected at 3 (E13) or 6 (E16) days post infection (dpi). Representative $TUNEL^+$ (green) stained placentas with DAPI to label nuclei taken (blue) at 100x magnification (A), with quantification of the percentage positive area (B). Placentas were immunostained for cytokeratin (red) to mark trophoblasts and DAPI (blue) to label nuclei (C) Representative images were taken at 20x magnification, with quantification of the percentage positive area (D). Placentas were

homogenized to measure concentrations (pg/ml) of IL-1β (E), IL-6 (F), and TNFα (G). Bars represent the mean ± standard error of the mean (n =5-9/group) with each symbol indicating one placenta and, for analysis of images, is the mean quantification of 6 fields of view. Significant differences ($p < 0.05$) were determined by unpaired two tailed t-test and are indicated by an asterisk (*). Scale bar: 50 µm

Figure 1.

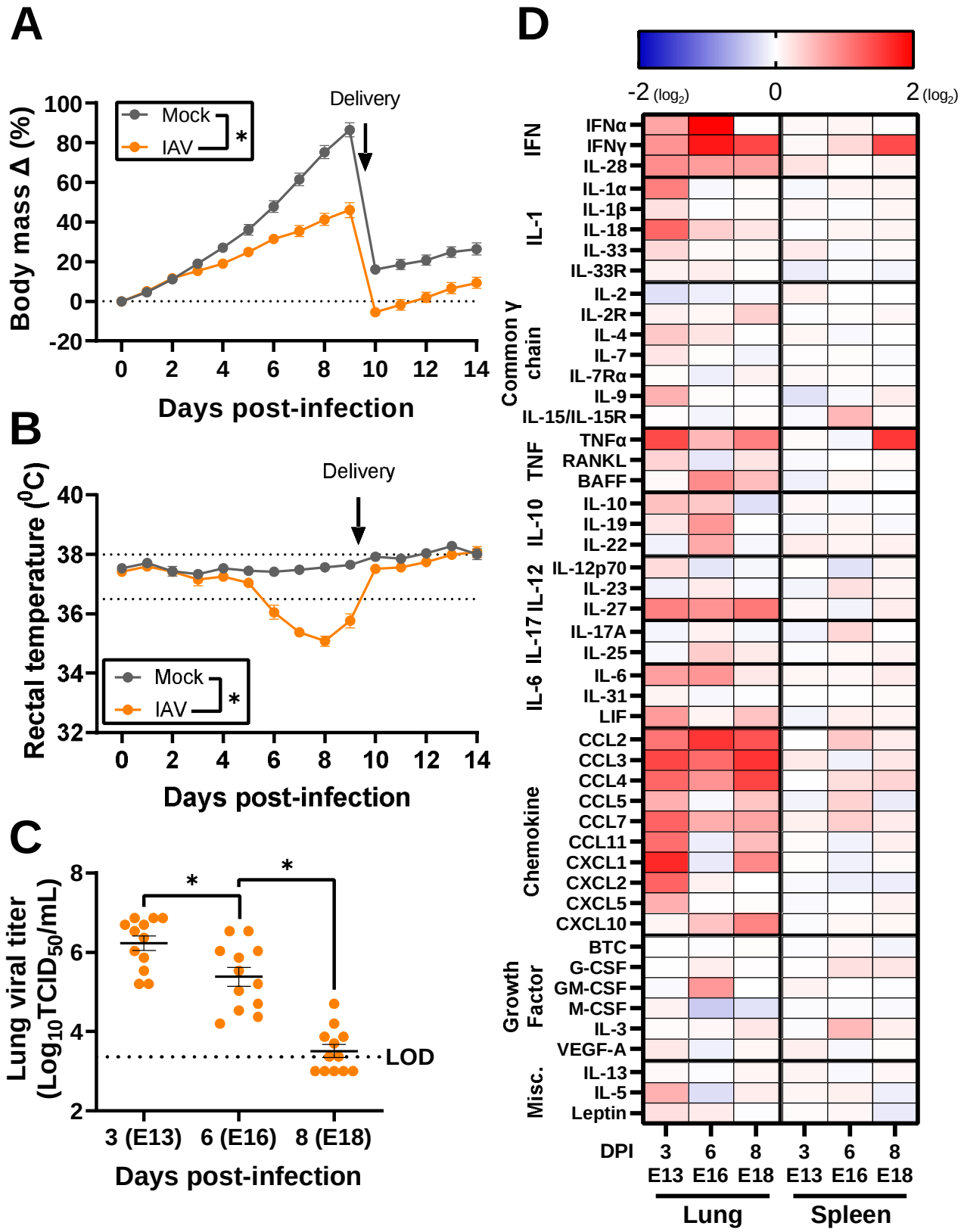
A
Body mass Δ (%)
Mock
IAV
*
Delivery
Days post-infection
B
Rectal temperature (⁰C)
Mock
IAV
*
Delivery
Days post-infection
C
Lung viral titer (Log10TCID50/mL)
*
*
LOD
3 (E13)
6 (E16)
8 (E18)
Days post-infection
D
-2 (log2)
0
2 (log2)
IFN
IFNα
IFNγ
IL-28
IL-1
IL-1α
IL-1β
IL-18
IL-33
IL-33R
Common γ chain
IL-2
IL-2R
IL-4
IL-7
IL-7Rα
IL-9
IL-15/IL-15R
TNF
TNFα
RANKL
BAFF
IL-10
IL-10
IL-19
IL-22
IL-12
IL-12p70
IL-23
IL-27
IL-17
IL-17A
IL-25
IL-6
IL-6
IL-31
LIF
Chemokine
CCL2
CCL3
CCL4
CCL5
CCL7
CCL11
CXCL1
CXCL2
CXCL5
CXCL10
Growth Factor
BTC
G-CSF
GM-CSF
M-CSF
IL-3
VEGF-A
Misc.
IL-13
IL-5
Leptin
DPI
3 E13
6 E16
8 E18
3 E13
6 E16
8 E18
Lung
Spleen

Figure 2.

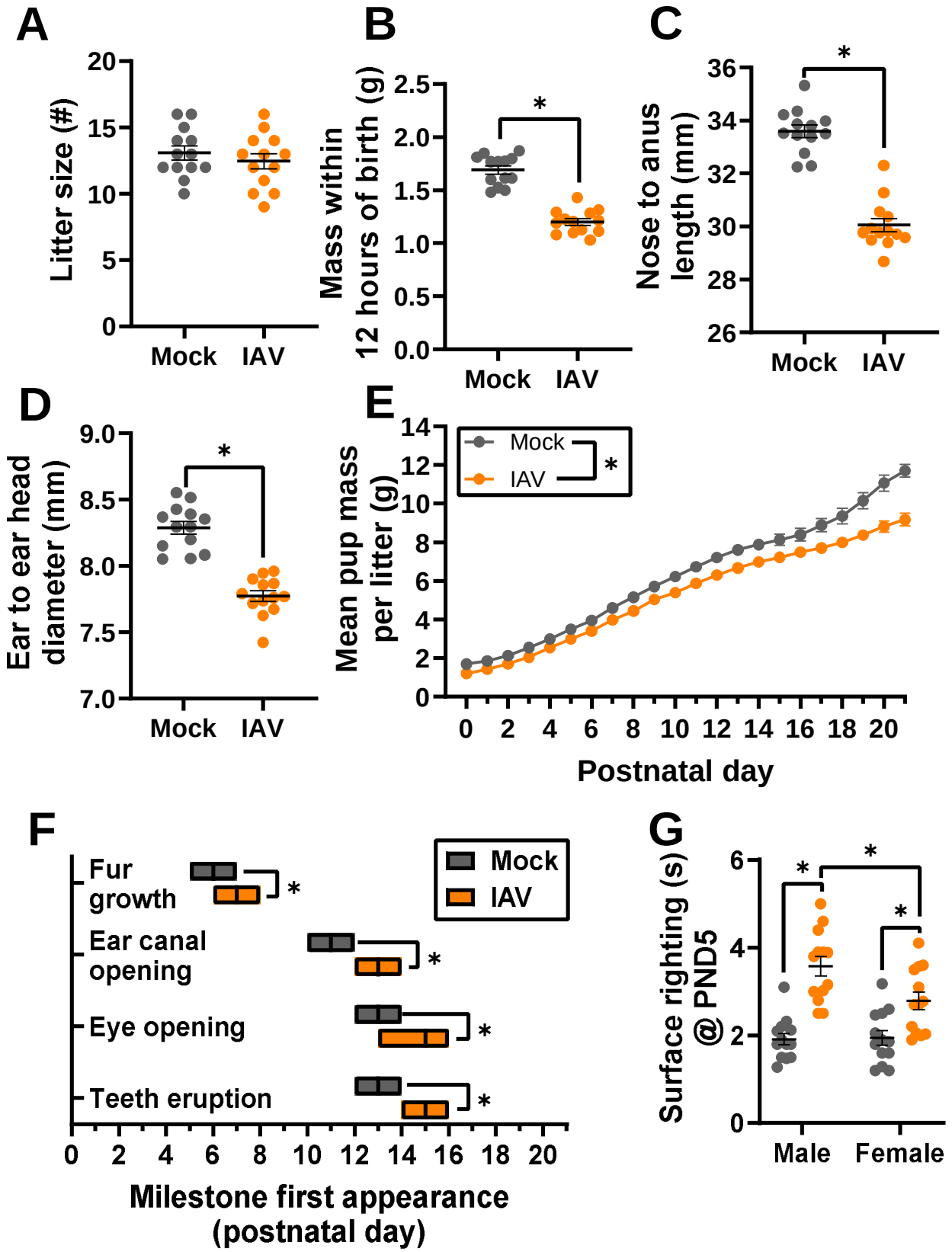
A
Litter size (#)
20
15
10
5
0
Mock
IAV
B
Mass within 12 hours of birth (g)
2.5
2.0
1.5
1.0
0.5
0.0
*
Mock
IAV
C
Nose to anus length (mm)
36
34
32
30
28
26
*
Mock
IAV
D
Ear to ear head diameter (mm)
9.0
8.5
8.0
7.5
7.0
*
Mock
IAV
E
Mean pup mass per litter (g)
14
12
10
8
6
4
2
0
Mock
IAV
*
0 2 4 6 8 10 12 14 16 18 20
Postnatal day
F
Fur growth
Ear canal opening
Eye opening
Teeth eruption
Mock
IAV
*
0 2 4 6 8 10 12 14 16 18 20
Milestone first appearance (postnatal day)
G
Surface righting (s) @ PND5
6
4
2
0
*
*
*
Male
Female

Figure 3.

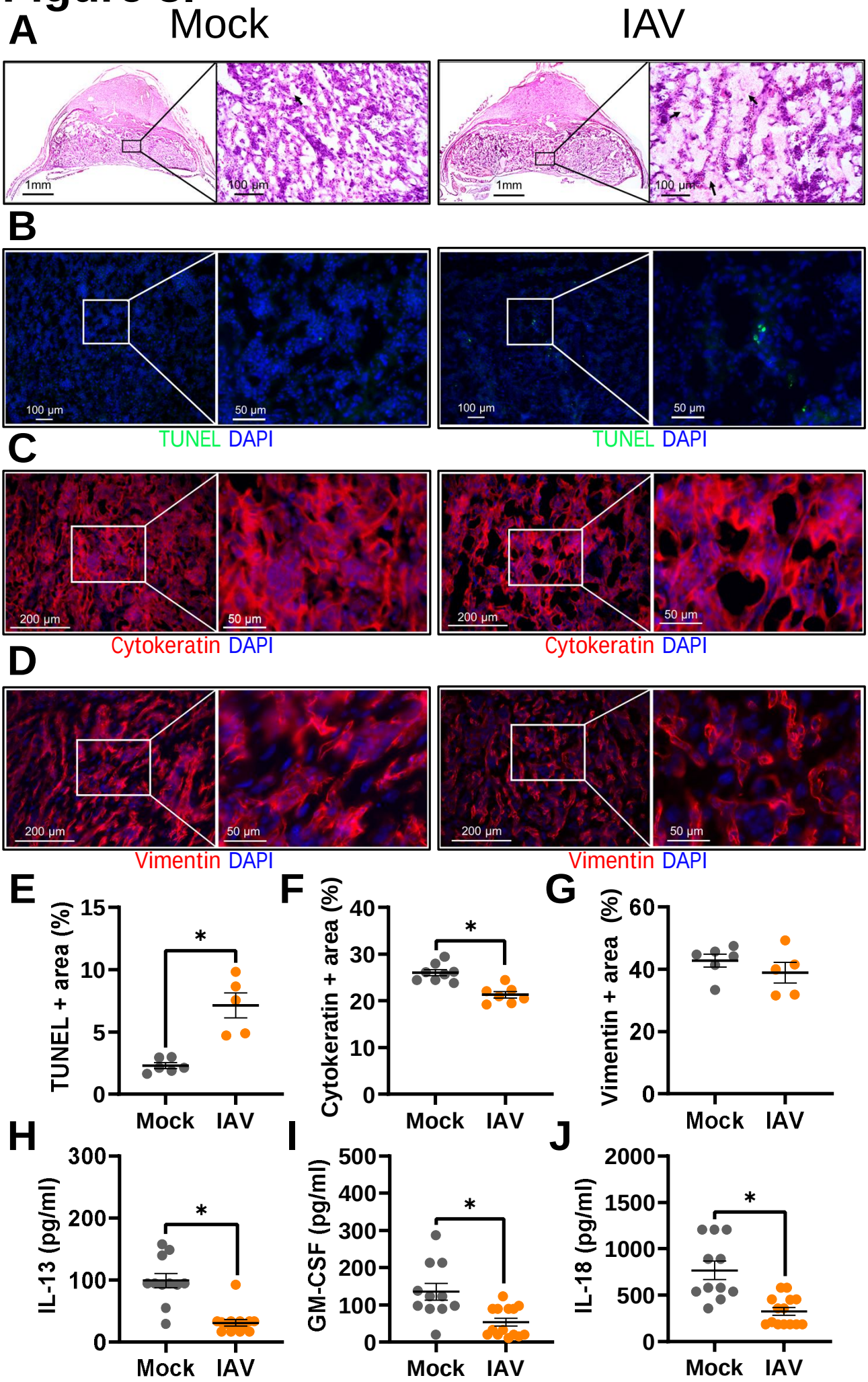
A
Mock
IAV
1mm
100 µm
B
100 µm
50 µm
TUNEL DAPI
C
200 µm
50 µm
Cytokeratin DAPI
D
Vimentin DAPI
E
TUNEL + area (%)
F
Cytokeratin + area (%)
G
Vimentin + area (%)
H
IL-13 (pg/ml)
I
GM-CSF (pg/ml)
J
IL-18 (pg/ml)
Mock
IAV
*

Figure 4.

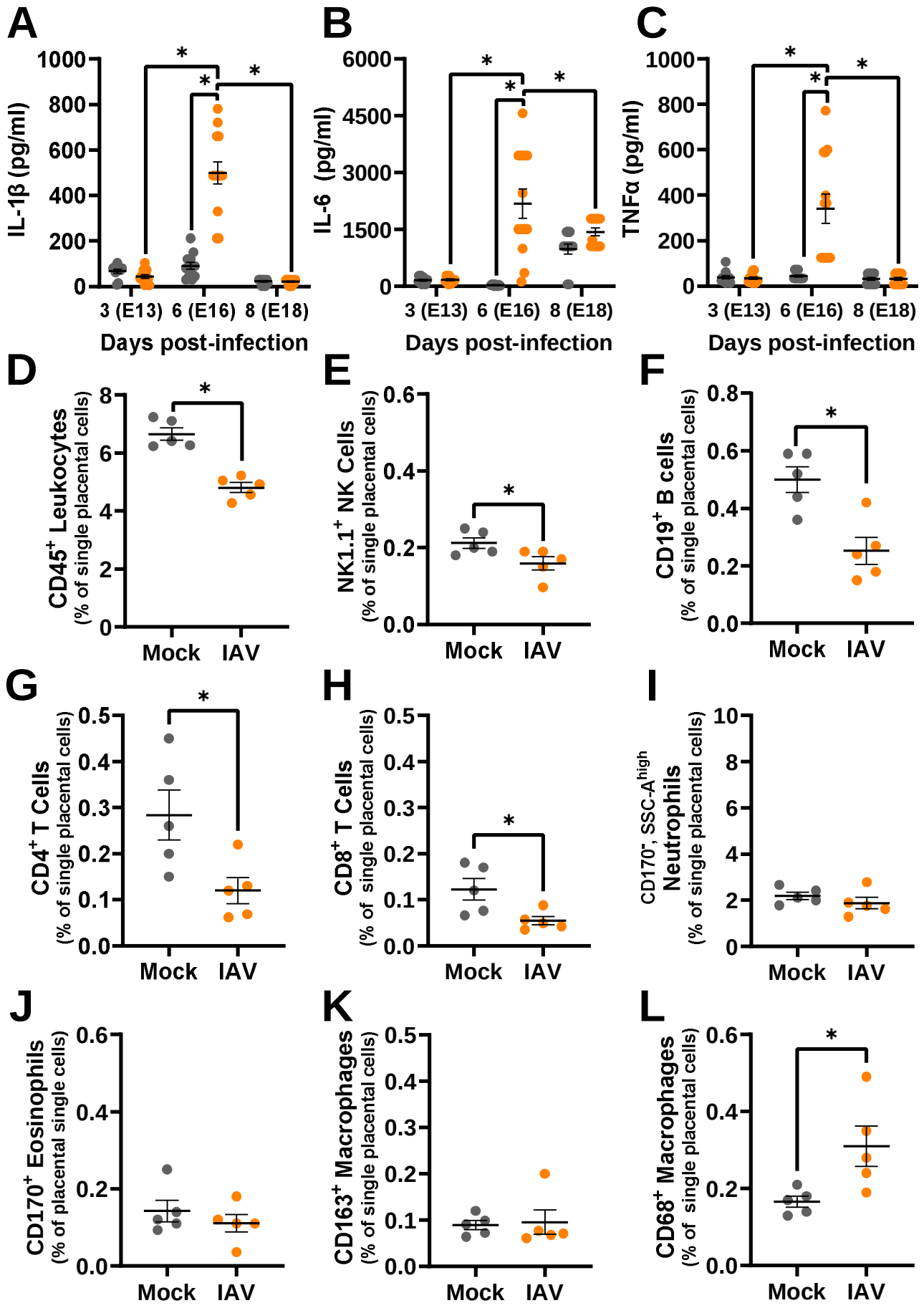
A
IL-1β (pg/ml)
1000
800
600
400
200
0
3 (E13)
6 (E16)
8 (E18)
Days post-infection
B
IL-6 (pg/ml)
6000
4500
3000
1500
0
C
TNFα (pg/ml)
D
CD45+ Leukocytes
(% of single placental cells)
8
6
4
2
Mock
IAV
E
NK1.1+ NK Cells
(% of single placental cells)
0.6
0.4
0.2
0.0
F
CD19+ B cells
(% of single placental cells)
0.8
G
CD4+ T Cells
(% of single placental cells)
0.5
0.3
0.1
H
CD8+ T Cells
(% of single placental cells)
I
CD170-, SSC-Ahigh
Neutrophils
(% of single placental cells)
10
J
CD170+ Eosinophils
(% of placental single cells)
K
CD163+ Macrophages
(% of single placental cells)
L
CD68+ Macrophages
(% of single placental cells)

Figure 5.

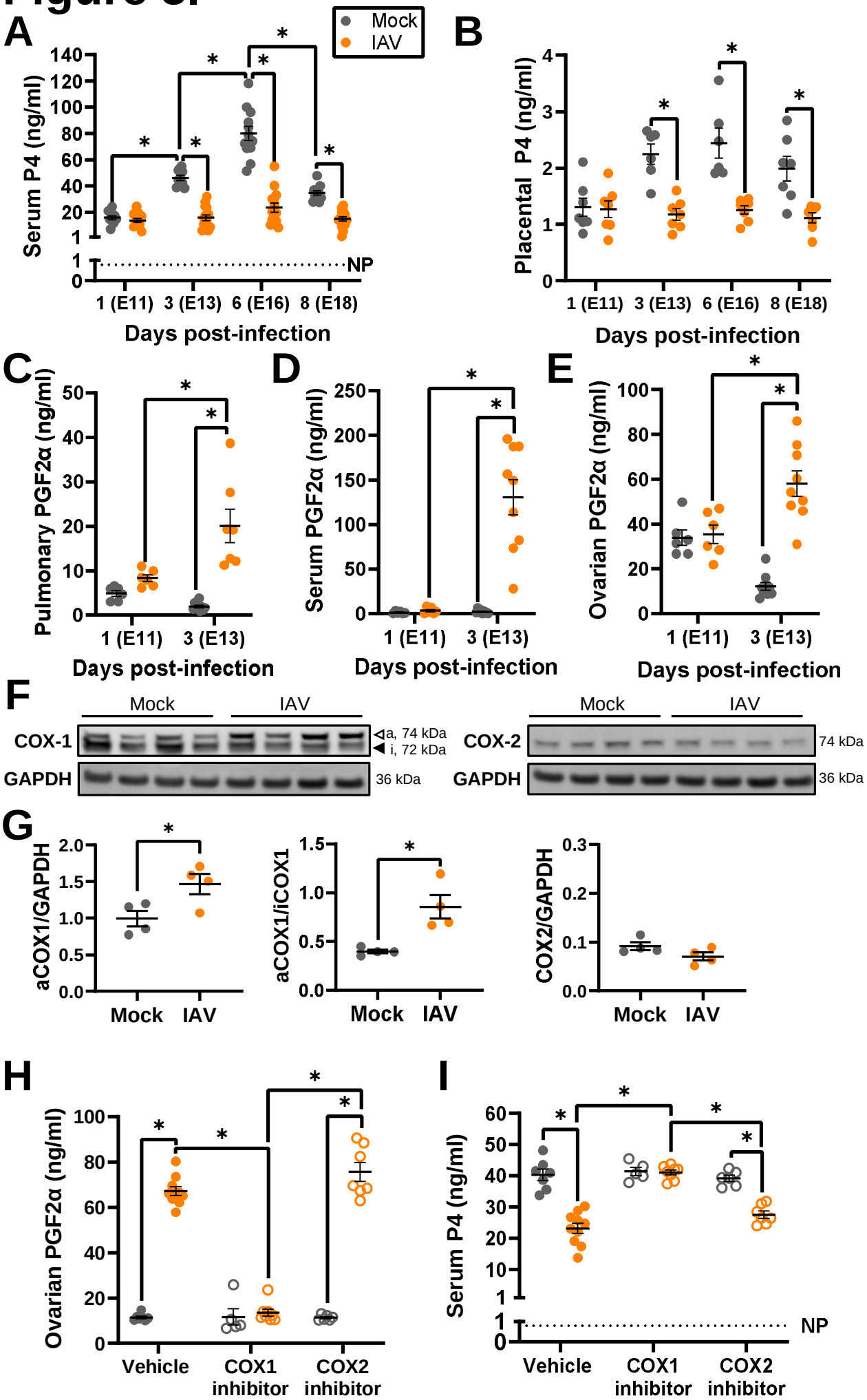
A
Mock
IAV
Serum P4 (ng/ml)
NP
1 (E11)
3 (E13)
6 (E16)
8 (E18)
Days post-infection
B
Placental P4 (ng/ml)
Days post-infection
C
Pulmonary PGF2α (ng/ml)
Days post-infection
D
Serum PGF2α (ng/ml)
Days post-infection
E
Ovarian PGF2α (ng/ml)
Days post-infection
F
Mock
IAV
COX-1
a, 74 kDa
i, 72 kDa
GAPDH
36 kDa
COX-2
74 kDa
G
aCOX1/GAPDH
aCOX1/iCOX1
COX2/GAPDH
H
Ovarian PGF2α (ng/ml)
Vehicle
COX1 inhibitor
COX2 inhibitor
I
Serum P4 (ng/ml)

Figure 6.

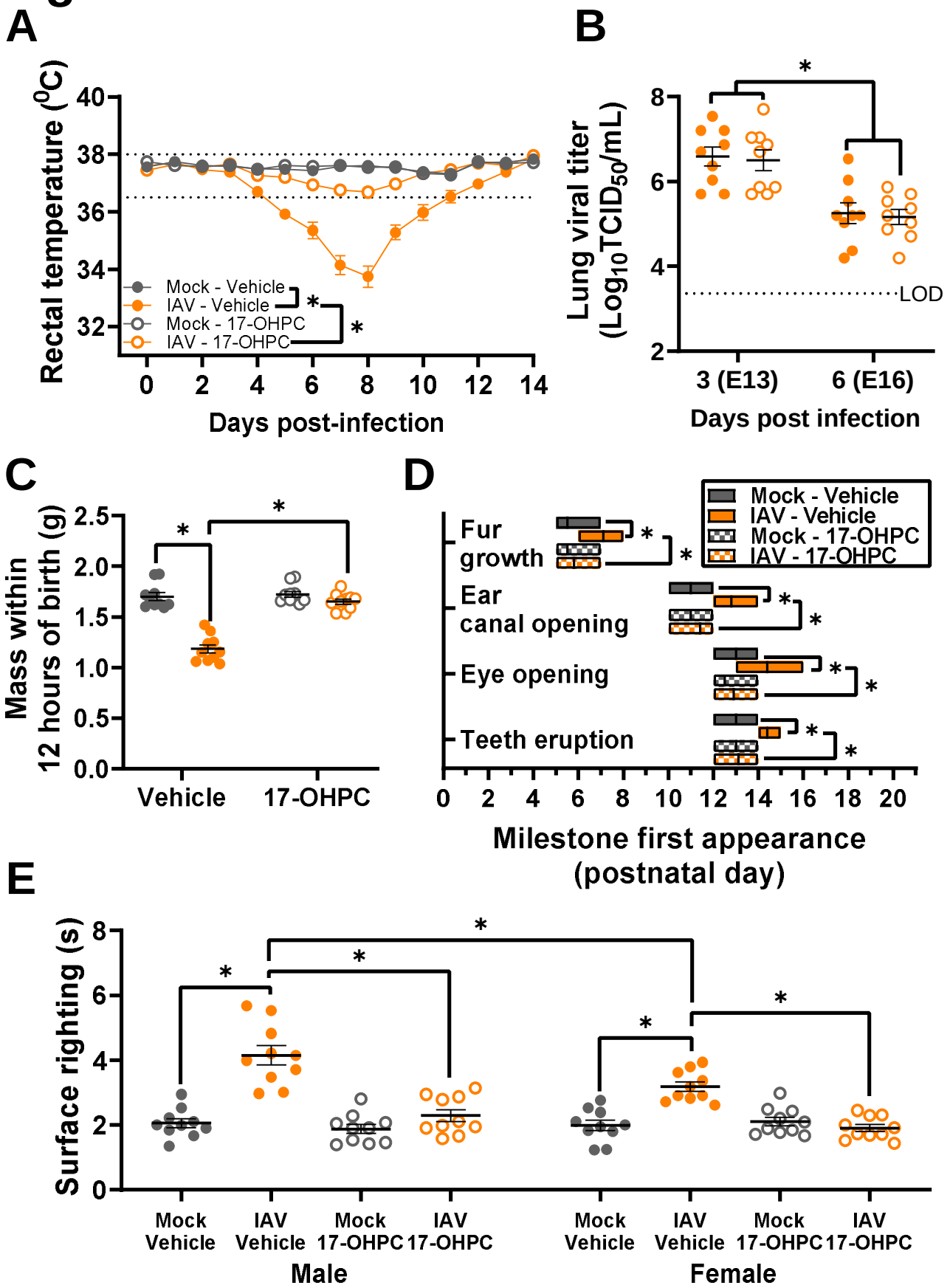
A
Rectal temperature (°C)
40
38
36
34
32
Mock - Vehicle
IAV - Vehicle
Mock - 17-OHPC
IAV - 17-OHPC
*
*
0
2
4
6
8
10
12
14
Days post-infection
B
Lung viral titer (Log10TCID50/mL)
8
6
4
2
*
LOD
3 (E13)
6 (E16)
Days post infection
C
Mass within 12 hours of birth (g)
2.5
2.0
1.5
1.0
0.5
0.0
*
*
Vehicle
17-OHPC
D
Mock - Vehicle
IAV - Vehicle
Mock - 17-OHPC
IAV - 17-OHPC
Fur growth
Ear canal opening
Eye opening
Teeth eruption
0
2
4
6
8
10
12
14
16
18
20
Milestone first appearance (postnatal day)
E
Surface righting (s)
8
6
4
2
0
*
*
*
*
*
Mock Vehicle
IAV Vehicle
Mock 17-OHPC
IAV 17-OHPC
Male
Mock Vehicle
IAV Vehicle
Mock 17-OHPC
IAV 17-OHPC
Female

Figure 7.

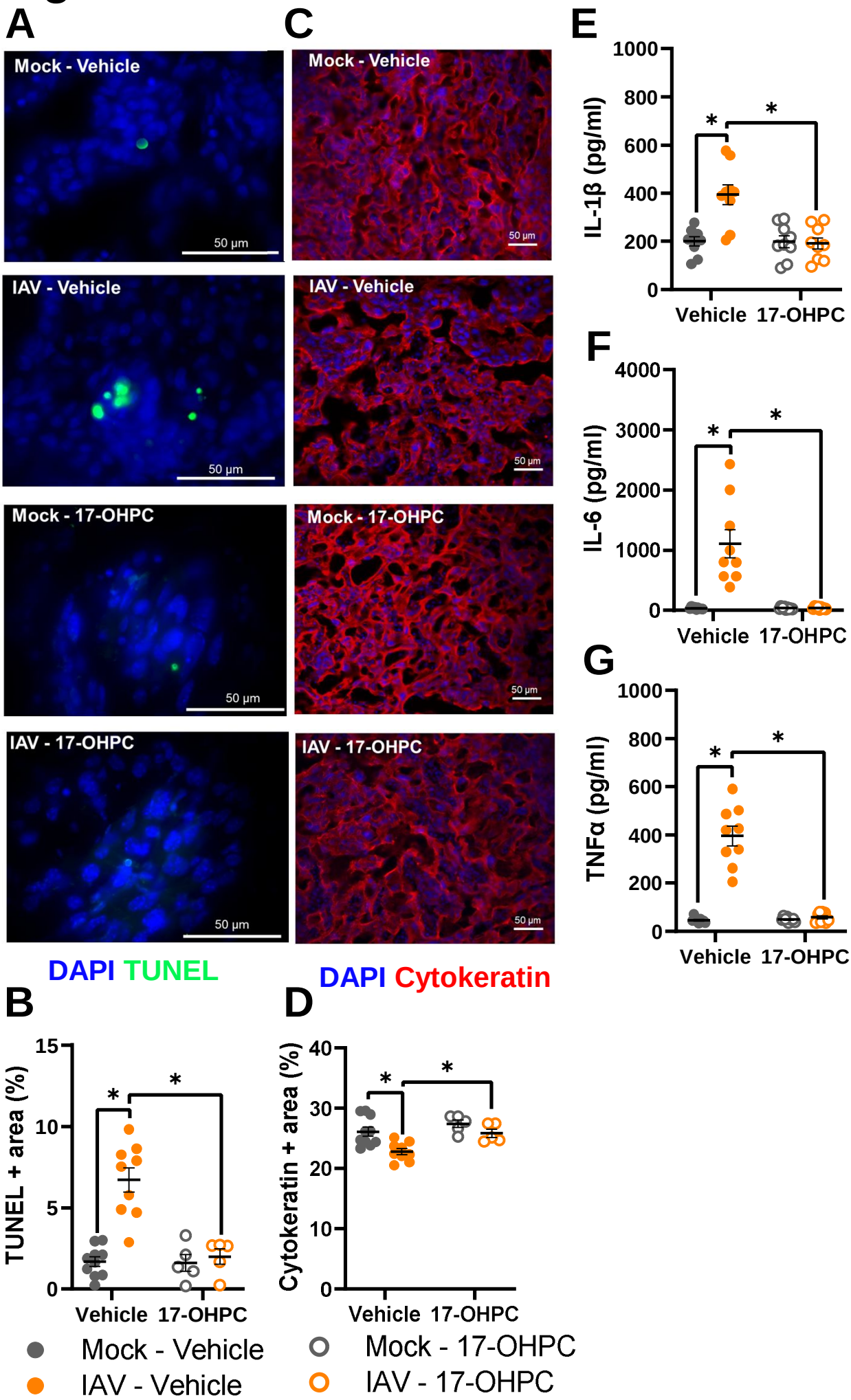
A
C
E
F
G
Mock - Vehicle
IAV - Vehicle
Mock - 17-OHPC
IAV - 17-OHPC
50 µm
DAPI TUNEL
DAPI Cytokeratin
B
D
TUNEL + area (%)
Cytokeratin + area (%)
IL-1β (pg/ml)
IL-6 (pg/ml)
TNFα (pg/ml)
Vehicle
17-OHPC
Mock - Vehicle
IAV - Vehicle
Mock - 17-OHPC
IAV - 17-OHPC